On Determining the Optical Constants of Sputtered U and a-Si at 304 and 584 Å

by

Matthew B. Squires

March 1999

Submitted to Brigham Young University in partial fulfillment of graduation requirements for University Honors

Advisor: David D. Allred Honors Dean: Steven E. Benzley

Signature: _____ Signature: _____

Abstract

The optical constants of uranium (U) and amorphous silicon (a-Si) at 304 and 584 Å in the extreme ultraviolet (EUV) are a source of error in the design of multilayer optics. Measured reflectivities of multilayer mirror coatings do not agree with calculated reflectivities using existing optical constants. The optical properties of materials depend on the electronic structure of the atom or compound being measured. In the low energy EUV it is uncertain how bonding affects the optical properties of elements and compounds. I have calculated the magnitude and the direction of the shift in the optical constants of U and a-Si from reflectivity measurements of DC magnetron sputtered U/a-Si multilayers at 304 and 584 Å. The reflectivity of the multilayers were measured using a UV hollow cathode plasma light source, a 1 meter VUV monochromator, a back-thinned CCD camera, and a channeltron detector. The reflectivities of the multilayer coatings were measured at 14.5 degrees from the normal surface of the mirror. The optical constants were calculated using IMD which uses CURVEFIT to fit the optical constants to reflectivity measurements of a range of multilayer mirrors that varied over a span of 150-250 Å layer thickness. The effects of surface oxide and roughness, interdiffusion, and interfacial roughness were numerically subtracted in fitting the optical constants. The optical constants at 304 Å of a-Si calculated from multilayers terminated with uranium oxide are $k = 0.037 \pm 0.015$, a positive 400% shift, and $n = 0.961 \pm 0.025$, a positive 3.5% shift, and the optical constants of U are $k = 0.67$, a positive 380% shift, and $n = 0.69$, a positive 2.4% shift. The refractive index at 304 Å of a-Si calculated from multilayers terminated with amorphous silicon is $n = 0.939$, a negative 1% shift, and the refractive index of U is $n = 0.705$, a positive 4% shift. The refractive index at 584 Å of a-Si calculated from multilayers terminated with amorphous silicon is $n = 0.806$, a positive 2% shift, and the refractive index of U is $n = 0.55$, a negative 6.8% shift. The refractive index at 584 Å of U calculated from multilayers terminated with uranium oxide is $n = 0.49$, a negative 17% shift. These shifts and magnitudes should only be used as the basis of further determination of the optical constants of U and a-Si at 304 and 584 Å.

Contents

1 List of figures

List of Figures

2 Introduction

On January 1, 2000 the IMAGE satellite will be launched to study the interaction between the magnetosphere of the earth and the solar wind. The magnetosphere is the boundary between magnetic field of the earth and charged particles coming from the sun, or the solar wind. It is hoped a better understanding of the "solar weather" and its interaction with the magnetosphere will help protect satellites and astronauts. One of the five instrument packages is going to use a telescope to image the shape of the magnetosphere by detecting the light that scatters from singly ionized helium (He^{1+}) trapped in the magnetic field of the earth. Singly ionized helium radiates light at 304 Å which is in the Extreme Ultraviolet (EUV) portion of the electromagnetic spectrum. The ionosphere of the earth also contains neutral helium that fluoresces at 584 Å. The 584 Å neutral He line can be up to five times more intense than the 304 Å He^{1+} line and is considered light pollution to the IMAGE satellite. The camera optics for the IMAGE satellite were designed to perform several functions. Primarily, they must reflect about 20% of the light at 304 Å. Light at 304 Å is not efficiently reflected by conventional optical coatings, like a single layer of gold or aluminum. But, 304 Å light can be efficiently reflected by a multilayer mirror coating. Another function of the mirrors was to not reflect more than 1% of 584 Å light coming from neutral He in the ionosphere. However, most materials reflect more than 10% at 584 Å, but a multilayer mirror can also be designed to not reflect light. A mirror coating that will not reflect over a range of wavelengths is called an anti-reflective coating.

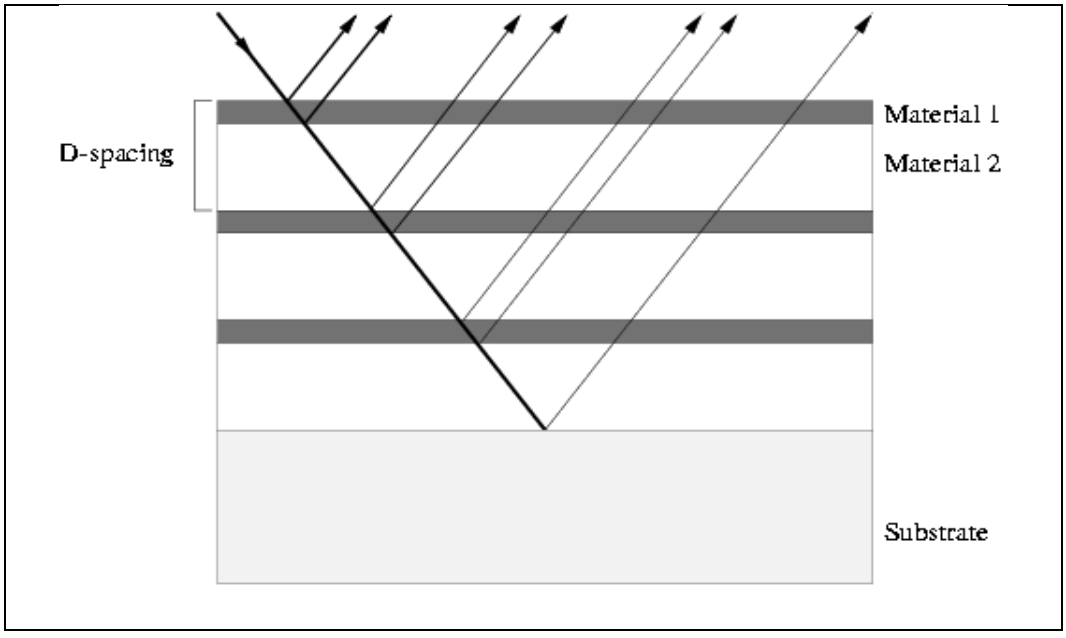

Figure 1: A Simple Multilayer

A multilayer is made by depositing alternating thin layers of different materials onto a substrate. Multilayers work on the principle of constructive and destructive interference of light reflecting from the multiple interfaces of a multilayer mirror coating. Multilayer mirror coatings have been made using various techniques and used for nearly a century. But a dual function multilayer that would reflect and antireflect at EUV wavelengths had never been made before.

Two factors determine how a multilayer mirror coating will respond at a wavelength of light: the optical constants of the materials and the total path-length the light will travel before exiting the multilayer. The optical constants of the materials used in the multilayer coating determine the percentage of light that will be reflected and transmitted from one interface. They also determine the wavelength of light inside of a material. The path length determines if light is reflected constructively or destructively after traveling through and reflecting from the different layers in the multilayer coating. The angle that light makes with the surface of the mirror coating and the thickness of the mirror coating determine the path length of the light through the mirror coating.

In preparation to submit a bid to make mirror coatings for the IMAGE satellite Dr. David Allred asked me to model plausible mirror coatings using LSMM [**?**]. LSMM uses a database of optical constants based on the revised Henke tables [**?**], however the Henke tables do not extend above ∼400 Å. An accurate model of a multilayer depends on knowing the optical constants at the wavelength of interest. There were few peer reviewed optical constants at 584 Å. There were published optical constants for many materials at 304 Å, but there was some doubt to the reliability of these optical constants. Some references had the optical constants above 400 Å [**?**, **?**] but when the data sets were merged they did not agree for many materials [**?**]. This meant there was some uncertainty and error in the existing optical constants in the EUV. This lack of optical constants proved to be one aspect of the contract that continued to hamper multilayer design for two years. Despite the lack of peer reviewed optical constants the existing optical constants at 304 Å and the best estimate of optical constants at 584 Å were used for many different elements to design optical multilayers. The resulting most probable combinations were uranium with aluminum or silicon.

A few mirror coatings for the IMAGE mission were designed using the best estimate of the optical constants of aluminum, silicon, and uranium at 304 and 584 Å. The preliminary designs were fine-tuned by making and measuring at 304 and 584 Å many permutations of the original designs. It was determined that the oxidation rate of aluminum was too high to be used for mirror coatings for the IMAGE mission [**?**]. Amorphous silicon was used in place of aluminum because it does not oxidize as readily and potentially passivates the surface of the multilayer mirror coating preventing the oxidation of the lower layers. Several other results were unexpected and gave more evidence that the optical constants in the EUV were not well known [**?**]. The measured reflectivity at 304 Å was slightly less than predicted even when roughness and interdiffusion were considered. The measured reflectivity at 584 Å was significantly less than calculated and was a very important factor in the completion of the IMAGE mirror contract. In the process of completing the IMAGE mirror contract a large number of multilayers coatings had been made that spanned a wide range of layer thickness. When the reflectivity measurements of the multilayer mirror coatings were compiled they could collectively be used to calculate the optical constants of U and a-Si at 304 and 584 Å.

3 Interaction of Light and Matter

3.1 Theory and Models

Quantum electrodynamics (QED) ultimately explains the interaction of light and matter, but the classical theory of electricity and magnetism adequately describes the steady state interaction of light and matter for the purpose of this thesis [**?**, **?**]. According to Maxwell's equations light is an oscillating electric and magnetic field propagating through space at a

constant velocity. The wavelength of light, λ, is determined by

$$\lambda = \frac{1}{\sqrt{\mu_i \epsilon_i}} \frac{2\pi}{\omega} \tag{1}$$

where μ_i is the permeability of the material and ϵ_i is the permittivity of the material. Both μ_i and ϵ_i depend on the medium the light is propagating through and ω in the angular frequency of the light. The subscript i is used to show that the wavelength of light depends on the material the light is propagating through. In a vacuum $\mu_i = \mu_0$ and $\epsilon_i = \epsilon_0$. In non-paramagnetic materials $\mu_i = \mu_0$. Iron, nickel, and cobalt are a few materials in that $\mu_i \neq \mu_0$. No paramagnetic materials are used for this thesis so it is assumed $\mu_i = \mu_0$. The value of ϵ_i depends on the electronic structure of the material the light is propagating through.

A model that works well to develop an understanding of how light interacts with matter is to assume an electron is harmonic coupled to a fixed nucleus. The electron is considered to be coupled to the nucleus by a spring with a spring constant of k_s (different than the wavenumber k). There will be a natural harmonic frequency ω_0 that depends on k_s. A physical interpretation of the spring is the coulombic force that binds the electron to the nucleus. There is also a damping force, γ, that is proportional to the velocity of the electron around the nucleus.

The frequency that the electron rotates around the nucleus depends on the distance from the nucleus. The distance of the electron from the nucleus is related to the energy of the electron while bound to the nucleus. The nucleus is assumed to be fixed and motionless and does not interact with light. The spacing of the nuclei determines the density of electrons in a material.

It is assumed that each electron in an atom has a resonating frequency, ω_0, that is associated with the energy of the electron in the atom. The energy and frequency of an electron can be can be calculated for many systems using QED. This energy can also be measured and calculated, but the determination of the energy of an electron in an atom will not be discussed in this thesis.

The interaction of light with frequency, ω, and a single electron with an oscillating frequency, ω_0, can be described by Maxwell's equations. The displacement of the electron by the electric field component of the light creates a dipole moment in the atom. The time-dependent dipole moment $\tilde{\mathbf{p}}(t)$ created by the movement of the electron is

$$\tilde{\mathbf{p}}(t) = \frac{(e^2)/m_e}{(\omega_0^2 - \omega^2 - i\gamma\omega)} \mathbf{E_0} e^{-i\omega t} \tag{2}$$

where m_e is the mass of an electron, e is the charge of an electron, γ is a damping factor, and $\mathbf{E_0}$ is the amplitude of the light's electric field. The bold face means the value is a vector and the tilde hat signifies the value is complex. In a real material electrons may oscillate at one of several different oscillating frequencies that are material specific. If there are N atoms per unit volume, and there is a fraction, f_j, of the electrons with frequency ω_j and damping factor γ_j the net polarization of the material is

$$\tilde{\mathbf{P}} = \frac{Ne^2}{m_e} \sum_j \frac{f_j}{(\omega_j^2 - \omega^2 - i\gamma_j\omega)} \tilde{\mathbf{E}} \tag{3}$$

where $\tilde{\mathbf{P}}$ and $\tilde{\mathbf{E}}$ are complex amplitudes. $\tilde{\mathbf{P}}$ and $\tilde{\mathbf{E}}$ are related by

$$\tilde{\mathbf{P}} = \epsilon_0 \chi_e \tilde{\mathbf{E}} \tag{4}$$

for an isotropic material. Isotropic means the polarization in the material is in the same direction as the electric field. There are many materials that are non-isotropic and require a more rigorous development [**?**]. The complex susceptibility, χ_e, is related to the complex permittivity, ϵ, by

$$\epsilon = \epsilon_0(1 + \chi_e) \tag{5}$$

By modeling the interaction of light with an electron in an atom as a damped harmonic oscillator, the complex permittivity takes the form

$$\epsilon = \epsilon_0 \left[1 + \frac{Ne^2}{m_e \epsilon_0} \sum_j \frac{f_j}{(\omega_j^2 - \omega^2) - i\gamma_j \omega} \right] \tag{6}$$

Even though ϵ is a complex number it is not written with a tilde because ϵ is explicitly complex. Following standard convention, the complex permittivity is expressed as ϵ_1 and ϵ_2. They are defined to be

$$\epsilon = \epsilon_1 + i\epsilon_2 = Re\{\epsilon\} + iIm\{\epsilon\} \tag{7}$$

The wave equation can still be solved with a complex ϵ and has a solution

$$\tilde{\mathbf{E}}(x,t) = \tilde{\mathbf{E}}_0 e^{i(\mathcal{K}x - \omega t)} \tag{8}$$

where $\mathcal{K}$ is the complex wavenumber that can be expressed as

$$\mathcal{K}^2 = \frac{\omega^2}{c^2} \left[1 + \frac{Ne^2}{m_e \epsilon_0} \sum_j \frac{f_j}{(\omega_j^2 - \omega^2) - i\gamma_j \omega} \right] \tag{9}$$

The wavenumber is often expressed in terms of the real and imaginary parts as

$$\mathcal{K} = k + i\alpha = Re\{\mathcal{K}\} + iIm\{\mathcal{K}\} \tag{10}$$

Because $\mathcal{K} = \frac{\omega}{c}\mathcal{N}$ the complex index of refraction is defined as

$$\mathcal{N} = n + ik = Re\{\mathcal{N}\} + iIm\{\mathcal{N}\} \tag{11}$$

Again $\mathcal{K}$ and $\mathcal{N}$ are complex but are not written with a tilde because they are explicitly complex. By noticing the similarity between equation (**??**) and equation (**??**), the roles of n and k can be explained by understanding the role of equation (**??**) in equation (**??**)

$$\tilde{\mathbf{E}}(x,t) = \tilde{\mathbf{E}}_0 e^{i(\mathcal{K}x - \omega t)} = \tilde{\mathbf{E}}_0 e^{-\alpha x} e^{i(kx - \omega t)} \tag{12}$$

The wavelength of a material can be expressed in terms of the wavenumber as

$$\lambda = \frac{2\pi}{k} \tag{13}$$

where k is the real part of the complex wavenumber. The imaginary part determines the opacity of the material to the frequency of light in question. Similarly, the real part of $\mathcal{N}$ is still known as the refractive index and the imaginary part of $\mathcal{N}$ is known as the extinction coefficient. In EUV and x-ray optics nomenclature $\beta = k$ and $\delta = 1 - n$. In the EUV and the x-ray portion of the spectrum the refractive index varies only slightly from unity so δ is commonly reported instead of n. It can be seen from equation (**??**) and equation (**??**) that $\mathcal{N}$ is determined by the electronic structure of the material in question.

Atomic scattering factors is another common way of describing the optical properties of a material [**?**]. Atomic scattering factors, f_1 and f_2, are used to report the optical properties of a specific material independent of density. The complex index of refraction can be calculated from atomic scattering factors assuming the density of the material is known. This is an important factor when designing mirror coatings that will be deposited via sputtering. Optical constants are most commonly measured from a bulk material of a known density. However, when a material, like crystalline Si (c-Si), is sputtered it is deposited in an amorphous state (a-Si). The density of a-Si is often 90% that of c-Si, but depends on the detail of deposition. Atomic scattering factors are used to compensate for the density of deposited materials without losing information about the overall electronic structure of the material. Atomic scattering factors are also used to estimate the optical constants of compounds by taking into consideration the optical response of each element in its stoichiometric amount and then scaling the optical response to the density of the compound. The results from this thesis will not be converted into atomic scattering factors because the densities of sputtered uranium and a-Si in the IMAGE multilayers are not known.

The model of an electron as a damped harmonic oscillator, as developed above, is a good model to show the relationship between the complex permittivity, wavenumber, and index of refraction. As mentioned previously QED and quantum mechanics gives an accurate description of how light interacts with matter. The details of how quantum mechanics could be used to calculate optical constants will not be explained in this thesis, but some of the model parameters from the previous example will be explained in terms of quantum mechanics [**?**]. The simple electron being bound by a spring can be described as a quantum harmonic oscillator that has discrete energy levels which can be approximated as

$$E = \sum_k (n_k + \frac{1}{2})\hbar\omega_k \tag{14}$$

where n_k is the occupational number of the mode with wavevector k. The occupational number determines the number of electrons at that particular energy. For a real system the energy levels would be given by a solution of the Hamiltonian with a Coulomb potential. The term f_j in equations (**??**) and (**??**) becomes the oscillator strength of an electron in a material. The oscillator strength is the measure of how one electron contributes to the overall response of the material to some frequency light. The polarization of the electron by the **E** component of the light wave can be described by a perturbation of the potential function. Time-dependent perturbation theory determines the probability that a photon of $\omega_{n'n} = (E_{n'} - E_n)/\hbar$ will be absorbed or emitted from the material, where n and n' are respectively the initial and final states of the electron. The absorption of light or damping by the material can be described by the electron relaxing to a lower state without coherent radiation of a photon. If no photon is emitted the energy must be dissipated by some mechanism, often by the creation of phonons, vibrations in the lattice structure of the material. The details of the relaxation of an electron to a lower state without radiation will not be discussed in this thesis.

3.2 Considerations in the EUV

The electronic structure of a material depends on the energies with which the electrons are bound to the nucleus and the bonds with the surrounding atoms. In x-ray physics this energy is largely determined by the total charge of the nucleus and the shell the electron is in. The optical constants of materials in the x-ray portion of the spectrum depend primarily on the core electrons. It is assumed the bonded valence electrons do not significantly effect the

inner electrons [**?**]. This assumption can only be made when the incident light is at a high enough energy that the energies of the valence electrons and their bonds are insignificant when compared to the energy of the light. It is generally supposed that above 100 eV the bonding of the valence electrons to the surrounding atoms does not significantly change the optical constants of the material.

In the visible and infrared portion of the spectrum the interaction of light with matter almost exclusively depends on the energetics of the valence electrons and neighboring structure. The bonds of the valence electrons with valence electrons in other atoms primarily determines the energy of a valence electron in a bulk material. The core electrons do not have a significant role other than shielding the charge of the nucleus. The oscillator properties of the core electrons are not significant to visible and other less energetic photons as is well documented in chemistry and molecular physics. The interaction of EUV light with matter lies somewhere between chemistry and physics. At high photon energies, excited core electrons dominate the optical properties of materials; in the visible and longer wavelengths the optical properties are largely determined by the energetics of the valence electrons in bonding orbitals. The optical properties of solids in the EUV seems to depend on the core electrons and bonding within the material. The EUV appears to be the region of transition where the assumptions made at high energies and those made at low energies are both significant factors [**?**]. The critical areas of transition are not well known but measurements in this thesis made at 584 Å suggests that 584 Å light is in this area of transition. The transition is not well documented because previously there has been little need to work in the EUV. The difficulties of sample preparation, theory, and measurement have not warranted the focus in previous years. The IMAGE mission was an opportunity to understand some aspects of optical constants in the EUV.

4 Deposition and Characterization

4.1 Deposition

All the mirror coatings for this thesis were made using a deposition method called sputtering. Sputtering has been used for 50 years as one method to deposit very thin coatings of a material on a substrate. Sputtering occurs when an energetic ion strikes the surface of a cathode and causes minute amounts of the target material to be ejected from the surface. This process was first discovered in high voltage cathode ray and x-ray tubes. For many years, it was only considered a negative parasitic effect, but it was later realized that the sputtering process could be used to make some thin films that were not possible using evaporation techniques of the time. Sputtering also made it possible to make thin films from alloys because the target does not need to melt to be deposited. It is hard to deposit two materials at the same time using evaporation because all materials evaporate from a molten mass at different rates, especially if one is refractory and the other is not. Using sputtering, both refractory and non-refractory materials are sputtered from the target at the same rate. It is also hard to make a multiple layered coating using evaporation because most of the material on the hot filament is deposited in one "shot".

Sputtering is usually done in a medium vacuum, 1×10^{-1} to 1×10^{-3} Torr (750 Torr = 1 atm), so the mean free path between molecules in the chamber is comparable to the distance to the substrate. At 1×10^{-6} Torr the mean free path is about one meter, and at 1×10^{-3} Torr, typical pressure for DC magnetron sputtering, the mean free path is about five centimeters [**?**]. Because the mean free path is comparable to the distance from the target to the substrate the ejected material can travel nearly unimpeded to the substrate. It is important the ejected material travels with few collisions to the substrate so the sputtered

material does not condense out of the gas phase and form atomic size granules that do not deposit smoothly. The higher the energy the ejected material strikes the substrate the better the coverage, density, and adhesion.

There are several ways to sputter materials but DC magnetron sputtering was used to deposit U and Si onto Si (100) substrates. DC sputtering uses DC power supplies that are less expensive than radio frequency (RF) power supplies and are less complicated. RF power supplies create electronic noise requiring special shielding to protect sensitive electronic devices used with sputter system. DC magnetron sputtering is more stable and robust than other deposition methods so it does not require as much effort to set up and maintain. DC magnetron sputtering of thick targets can only be achieved with materials that are reasonably conductive and non-ferromagnetic. Uranium and silicon are both conductive and non-ferromagnetic, and therefore, can be efficiently sputtered with a DC magnetron sputterer.

Before sputtering begins, the deposition chamber is evacuated to a pressure less than 10^{-6} Torr to remove nitrogen, oxygen, and water vapor. These gases are removed to prevent the formation of nitrides and oxides in the deposited film that will change the optical properties of the materials being deposited. The presence of these gases can also change the final thickness of the deposited films. Water vapor is the most difficult contamination to remove from the deposition chamber. While the deposition chamber is constantly being evacuated by a cryopump it is heated to greater than 100 ^{o}C for an hour with heating tape to speed the removal of water vapor, and is then allowed to cool to room temperature. The partial pressures of water and nitrogen in the system were typically less than 10^{-6} Torr before deposition. The partial pressures of all the gases in the deposition chamber were measured using a quadropole residual gas analyzer (RGA).

Deposition can begin after the base pressure in the chamber is 3×10^{-6} Torr or lower, this takes approximately three to four hours of pumping time. After the base pressure has been reached the entrance to the vacuum pump is mostly blocked or throttled. The pressure in the deposition chamber rises to 3-7$\times10^{-6}$ Torr after the entrance is throttled. Argon is then added to the system to a pressure of 1-2$\times10^{-3}$ Torr. Argon is used to create a plasma because is least expensive of the nobel gases, has a large enough mass to efficiently eject material from the surface of the target, and readily forms a plasma. Nobel gases are used for sputtering because they do not form compounds with other materials. The argon partial pressure in the deposition chamber is maintained by a mass flow controller and is monitored by the RGA. Ultra high purity (99.999% pure) argon is used to lessen the number of contaminants in the chamber, however the partial pressure of nitrogen rises to 1% of the argon pressure as measured by the RGA.

The plasma is created using a DC plasma power supply capable of creating a 1000 volt potential between the target and the dark space shield. The plasma is initiated by a random event, like a cosmic ray or radioactive particle, ionizing an argon gas atom near the target. The electric field created by the potential difference maintains the plasma by accelerating ions and electrons in the chamber. Positive argon ions are accelerated towards the target and the electrons are accelerated to the rest of the system that is grounded. There is a probability that the electrons will ionize other gases in the chamber before striking the walls of the chamber. The plasma is held close to the surface of the target and the time of flight of the electrons is increased by strong permanent magnets directly below the target. When an electron is ionized from an argon atom it is trapped by these magnetic fields. An electron moving in a magnetic field will execute cycloidal motion in the magnetic field according to

$$F_B = m_e e(\vec{v} \times \vec{B}) \tag{15}$$

The time an electron is moving inside the chamber, and the time it has to ionize other

atoms, is significantly greater because it moves in a spiral motion above the target. This spinning motion increases the probability that an electron will ionize argon atoms close to the surface of the target. The plasma is largely maintained by the energetic electrons in the sputter chamber. The electron population is maintained by the ionization of argon atoms and by the ejection of electrons when an argon ion strikes the surface of the target.

Because argon ions are positively charged they are accelerated toward the target that is maintained at a negative potential. When an argon ion strikes the surface of the target material there is a significant probability it will eject one or more atoms of the target material from the target surface. Argon is a nobel gas and does not form compounds with other elements so it is assumed the target material is the same composition when it strikes the surface of the substrate. Some of the sputtered material will impinge on the surface of the substrate and will stick to the substrate. The thickness of the deposited material can be controlled to a atomic dimensions because the deposition occurs on the atomic level. The thickness of an individual layer is determined by the time the substrate is held over a target.

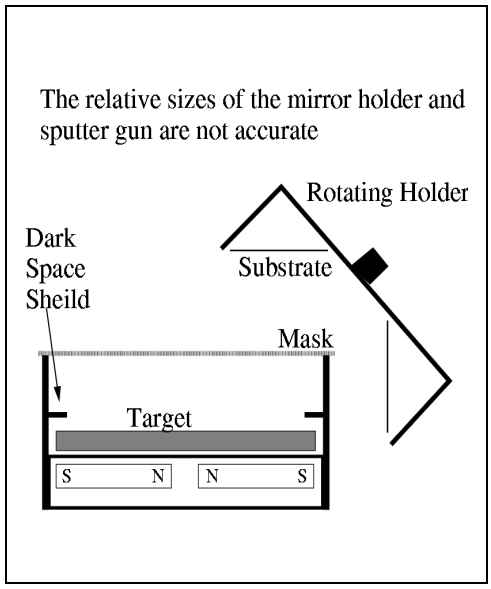

Figure 2: Side View of Sputter Setup

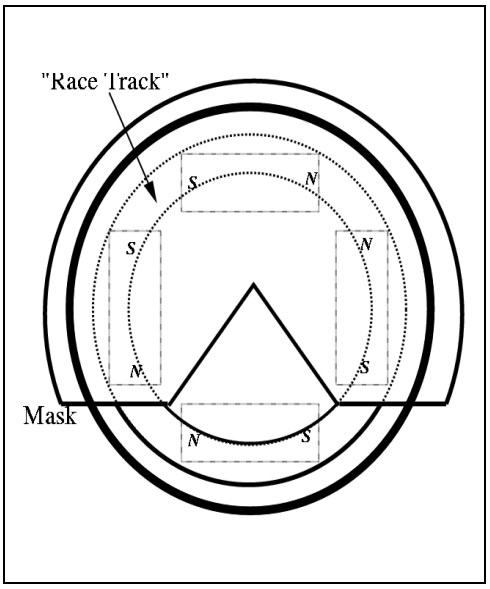

Figure 3: Top View of Sputter Setup

The atoms of the target material leave the target at very high velocities ($\sim$ 3000 m/s) and travel in all directions until they strike a surface. The density that the atoms arrive at the substrate can roughly be estimated by the cosine from the center of the substrate. A $\cos\theta$ distribution is accurate for a point source, but the targets are five inches in diameter and the surface of the target is unevenly eroded after many sputter runs. The electrons are confined close to the surface of the target to improve sputter rates, but the electron density varies over the surface of the target. Because of this variation the region toward the outside of the target tends to be sputtered more rapidly than the center. This creates a "racetrack" (see figure **??**) that also affects the distribution of the atoms coming from the target. The exact distribution was not calculated because uniformity could be effectively achieved otherwise. Uniformity over the surface of the substrate was obtained by spinning the substrate over the target. Part of the target area was blocked off or "masked" to achieve better uniformity. The uniformity was optimized experimentally by measuring the thickness by x-ray diffraction. The area and position of the masks and sputter times were adjusted to increase uniformity. The mirrors were held at an 14.5^o in a specially designed substrate

holder made for the IMAGE mission. This holder was designed to hold flat test mirrors along the chord of a curved mirror if it was held by a different substrate holder (see figure **??**). Flat samples were used to test the uniformity and thickness because they could be measured by x-ray diffraction. Curved mirror substrates could not be easily measured using the existing x-ray disfractometer.

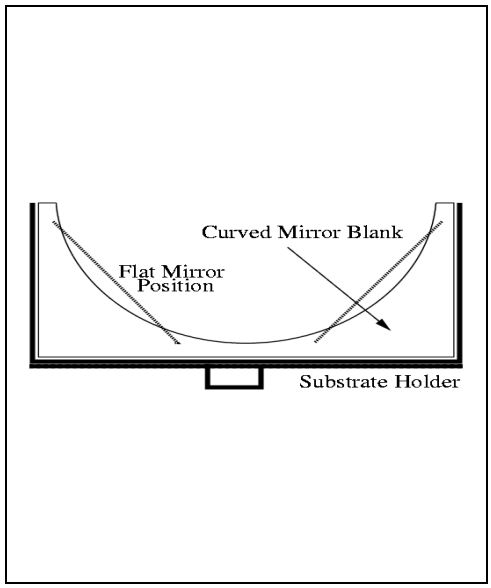

Figure 4: Relative Positions of Flat and Curved Substrates

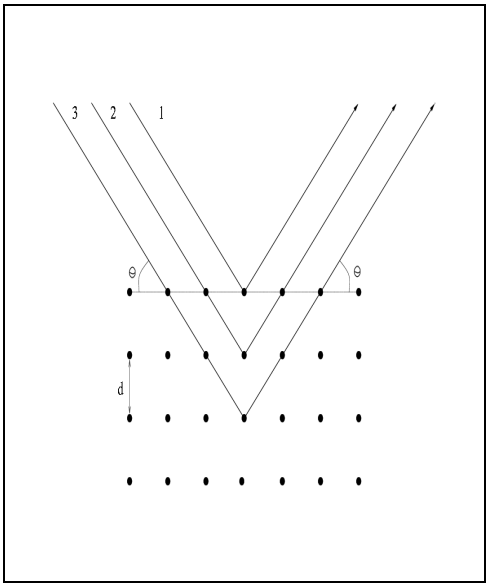

Figure 5: Bragg Diffraction

4.2 Characterization with x-rays

The thickness of the multilayer mirrors was determined using x-ray diffraction as previously mentioned. Bragg's equation of diffraction from a crystal states

$$2d \sin \theta_m = m\lambda \tag{16}$$

where d is the spacing between crystals, θ_m is the angle that corresponds to an interference peak, λ is the wavelength of light in the material, and m is the order number of the interference peak. This equation was derived to describe diffraction from crystals but Bragg's equation can be used to describe diffraction from any periodic structure that has a thickness on the order of the light used to measure the sample. Bragg's equation can give a good estimate of the thickness of a multilayer film, but the Fresnel equations must be used to calculate the thickness more accurately. IMD and LSMM based on the Fresnel equations provide an accurate model to determine the thickness of the multilayer period. In the geology department at BYU there is a Scintag x-ray disfractometer that was used to determine the thickness of the period of the multilayer coatings. The spatial uniformity was also determined by measuring the thickness of a multilayer coating at various places on a sample. When optimized the sample thickness varied about 1% over five centimeters along the radius of the sample. The ratio of the top layer thickness to the thickness of an entire period, Γ, was determined by fitting the relative peak heights to a model using LSMM or IMD. All the multilayers used in the calculation of the optical constants had a Γ of 0.7 ± 0.03.

5 Reflectivity Measurements and Analysis

5.1 Equipment Setup

Most optical constants in the EUV are measured using either a synchrotron or with a laser plasma source coupled with an appropriate detector. These light sources are very expensive to run and maintain, and are normally optimized to measure reflectivity or transmission in the high-energy portion of the EUV to high energy x-rays. BYU has a measuring system that can be operated at a relatively low cost, and is optimized to measure in the lower energy portion of the EUV. This system cannot replace a synchrotron or laser plasma system, but it can be used to make measurements in the low energy portion of the EUV.

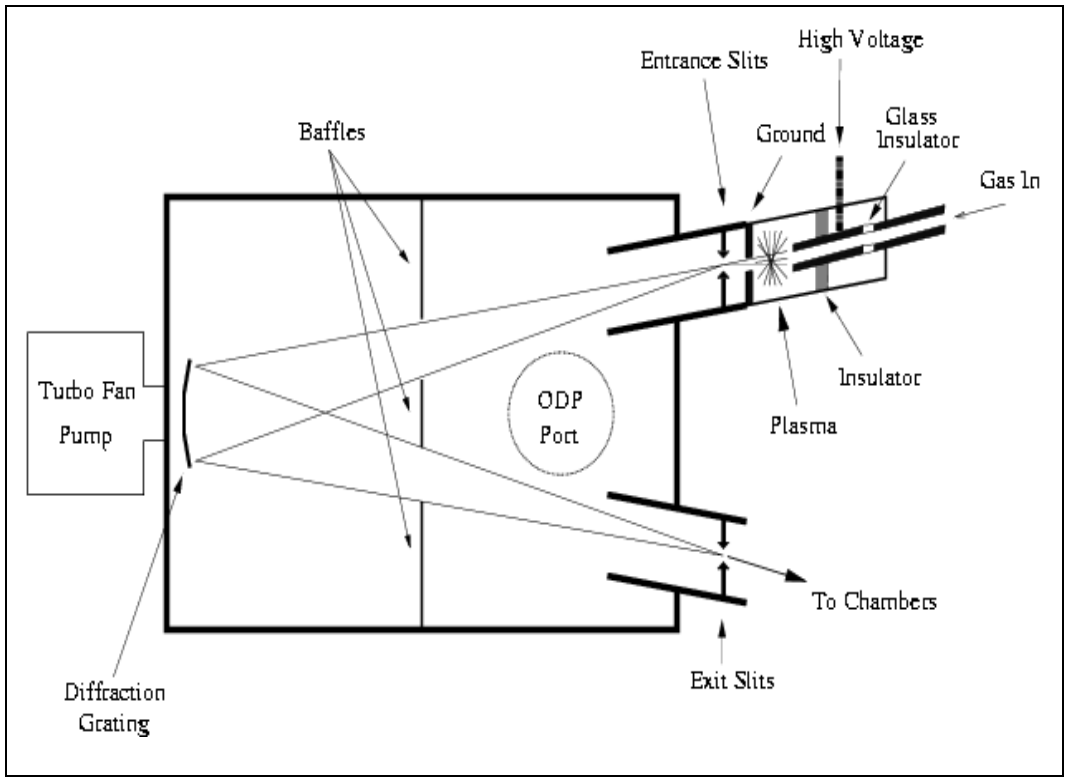

Figure 6: Overall Setup

As represented in figure **??** light is created in the plasma lamp, and passes through a set of slits. The light then passes through a baffle, and reflects off a curved diffraction grating that can be positioned to select one wavelength of light. The light then passes through another baffle and then exits another set of slits. The light can then be reflected off a mirror and into a detector, or the light can be directly measured to monitor the intensity of the plasma lamp. The system is evacuated by a vacuum pump mounted directly below the monochromator chamber, or behind the diffraction grating.

6 Vacuum System

The measurement system is operated under vacuum at less 1×10^{-4} Torr because EUV light is strongly absorbed in air and the channeltron detector would arc if operated above 1×10^{-4} Torr. The system was originally evacuated by an oil diffusion pump (ODP) mounted directly below the monochromator chamber. The rest of the system was protected from diffusing oil by a chilled chevron baffle directly above the ODP. The ODP was removed because it was continually broke down and there was some evidence the coolant for the ODP and the chilled baffle was leaking into the vacuum.

The ODP was replaced by a 46k RPM turbo molecular pump that could be operated without oil or a chilled baffle. This pump was mounted directly behind the diffraction grating where it could be removed and replaced easily. The detector chambers were evacuated through the exit slits and by a separate 56k RPM turbo molecular pump to assure the detectors could be operated safely.

6.0.1 Hollow Cathode Plasma Lamp

A McPherson hollow cathode plasma lamp was used to produce UV light. The plasma is made by flowing different gases in a region of high potential difference. The process of igniting and maintaining a plasma in the plasma lamp is very similar to the process explained in section **??**. There are no magnets in the plasma lamp so the plasma is not confined to any region of the plasma lamp. The pressure in the plasma lamp is on the order of 10^{-1} Torr, about one hundred times the pressure in the sputtering chamber. The plasma is easily maintained because, the probability of collisions between particles is greater at higher pressures. The plasma is still maintained by the acceleration of the electrons in the electric field, but EUV light is created by collisions of gas atoms with electrons or other ionized gas atoms. These collisions impart energy to the electrons in the gas atoms. If there is enough energy the electron can be excited to a higher energy level in the atom. Because there is a vacancy in a lower energy level the electron may decay to the lower energy. This decay is governed by selection rules, the dipole transition is the most dominant selection rule. This means that nearly all of the transition will change angular momentum or quantum number ℓ by $\pm$ 1.

Helium gas was used to produce light at 584 and 304 Å. Neutral helium has two electrons in the 1s shell. When an electron is excited to the 2p state and decays to the 1s state it will radiate light at 584 Å. This is a very intense spectral line because it does not need a lot of energy to be excited, the helium atom does not have to be ionized, and the 2p-1s is a probable transition. The 304 Å line is created by the 2p–1s transition in a singlely ionized helium atom. This spectral is not as bright because it needs more energy to excite the electron to the 2p state, it depends on the percent ionization of the helium gas, and it is not as probable as the 2p–1s transition.

The hollow cathode is powered by a Universal Voltronics Co. high voltage DC source capable of producing greater than 1kV and greater than 1A, but was never run higher than 1kV and 1A. The hollow cathode lamp was used in series with a combination of high power ballast resistors to regulate the current through the hollow cathode (figure **??**). All the ballast resistors are 2000 $\pm$ 10 Ω and were purchased from Cesiwid Inc. Four resistors were used in a parallel/series combination with two sets of parallel resistors that were is series with a total resistance of 2000 Ω, and are able to dissipate four times the power of any one resistor.

The current through the hollow cathode was measured to monitor the stability of the plasma lamp. The steady state current through any closed DC loop will be zero. This

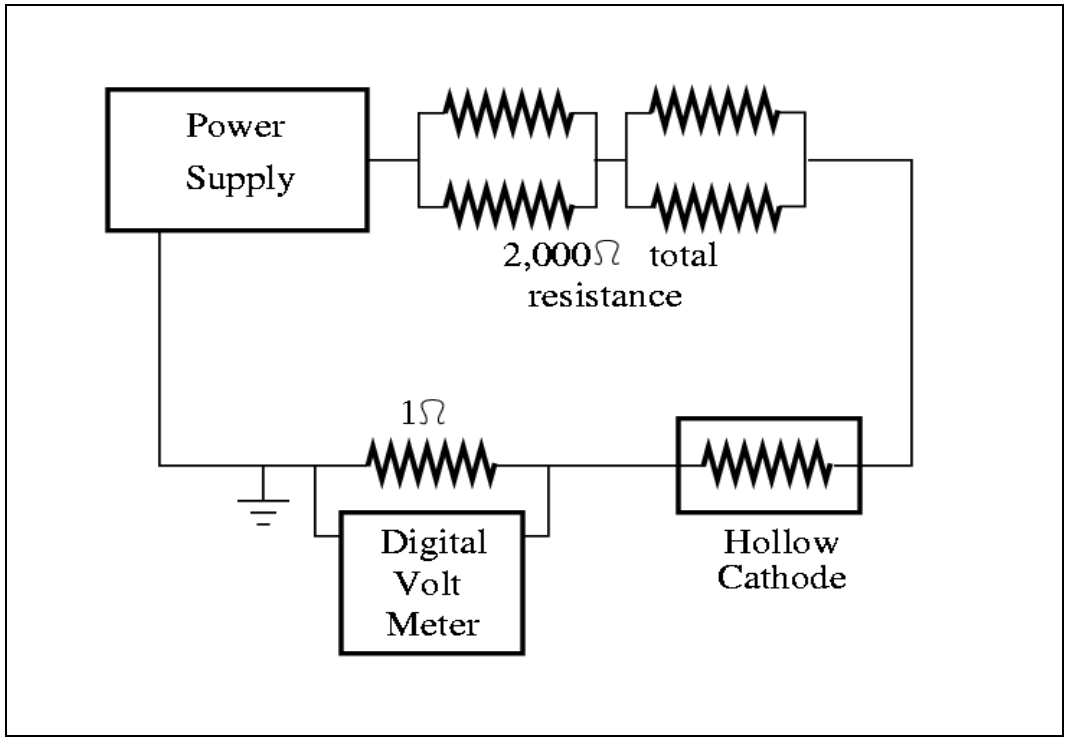

Figure 7: Electric Diagram

means the current measured in any part of the loop will be the same as the current through the plasma lamp. A 1Ω resistor was put in series with the plasma lamp to monitor the current. The current was measured on the low voltage side of the plasma lamp for safety reasons (figure **??**). The current was determined by measuring the voltage difference across the 1Ω resistor, according to Ohm's law

$$I = \frac{V}{R} \tag{17}$$

The voltage difference was measured by a Keithley 2000 digital multimeter. Measuring the current gave some clues to the stability of the plasma lamp, but it was not a sure sign that the light emission is stable. I observed the intensity of the light from the plasma lamp varied greatly but the current remained nearly the same over hours of continuos running. A low current despite high voltages is a sign that the plasma lamp needs to be cleaned.

The benefits of using the hollow cathode plasma lamp are: it is relatively inexpensive to operate and repair, it can be run for months without cleaning, and it does not require any special tools to repair. The disadvantages of using the plasma lamp are: it uses a plasma (which is intrinsically unstable) to create light, there are spatial variations in the intensity of the emitted light, and these spatial variations depend on the wavelength of light being monitored.

6.0.2 McPherson Monochromator

The McPherson scanning monochromator is used to select one spectral wavelength of light so measurements can be made at one specific wavelength. The McPherson monochromator

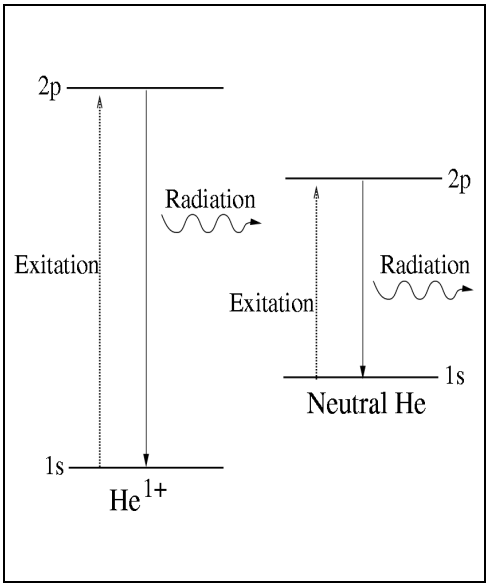

Figure 8: Atomic Transitions

Figure 9: Cross Section of Plasma Lamp

can also scan smoothly through many wavelengths of light making it possible to measure the reflectivity of a sample over a range of frequencies of light. The monochromator can produce light from about 300 to 1000 Å, and control the wavelength of the light to about 0.25 Å. This precision is determined by the mechanism that controls the diffraction grating. The dial controlling the grating is marked ever angstrom and the position can be estimated to about $1\backslash 4^{th}$ of a division. The diffraction grating determines the range of light the monochromator can produce. A special reflection grating with a platinum coating and a blaze angle optimized for 420 Å light was used to produce light at 304 Å. The platinum coating is essential for measurements in the EUV because the standard MgF_2 coating on most diffraction gratings attenuates nearly all EUV light below 500 Å. A reflection grating works much like a transmission grating. The equation for response from a diffraction grating is

$$d \sin \theta_m = m\lambda \tag{18}$$

where d is the spacing between the lines on the diffraction grating, θ_m is the angle the light leaves the grating, m is the order number of the light, and λ is the wavelength of the light. If the grating is held at a specific angle the wavelength coming from the grating can be determined. This concept is used to select one wavelength of light from light that contains many wavelengths.

It is presumed the light coming off the grating is nearly unpolarized. In general, the amount light polarizes depends on the angle of incidence. Light tends to polarize less when it reflects close to normal incidence, and the polarization effect is not as pronounced in the EUV as it is in the visible. Light from the entrance slits reflects at 15^o from normal on the grating.

The beam of light reaching the sample is defined by adjustable entrance and exit slits. The vertical slits can be adjusted by a moving a dial below each slit, the dial extends out of the vacuum chamber so the slits can be changed when the system is under vacuum. The vertical slits were 50–300 microns depending on the intensity of the light, and can be made as small as twenty microns. The horizontal slits can be adjusted by loosening set screws

and then adjusting the slits by hand when the detector chambers are removed. The width of the horizontal slits can be adjusted to approximately 0.1 cm. The horizontal slits were normally one centimeter in width, and were changed infrequently.

6.0.3 Measurement Chambers

Two chambers were used to measure the reflectivities of multilayer coating. Chamber 1 was used to measure the absolute reflectivity of a multilayer coating, and could only measure the reflectivity of one mirror coating at a time. Chamber 2 was used to measure the relative reflectivity of three mirrors to a known reference mirror. Chamber 2 was primarily used to measure the relative reflectivity of multilayer mirror coatings because measurements could be made significantly faster than using chamber 1.

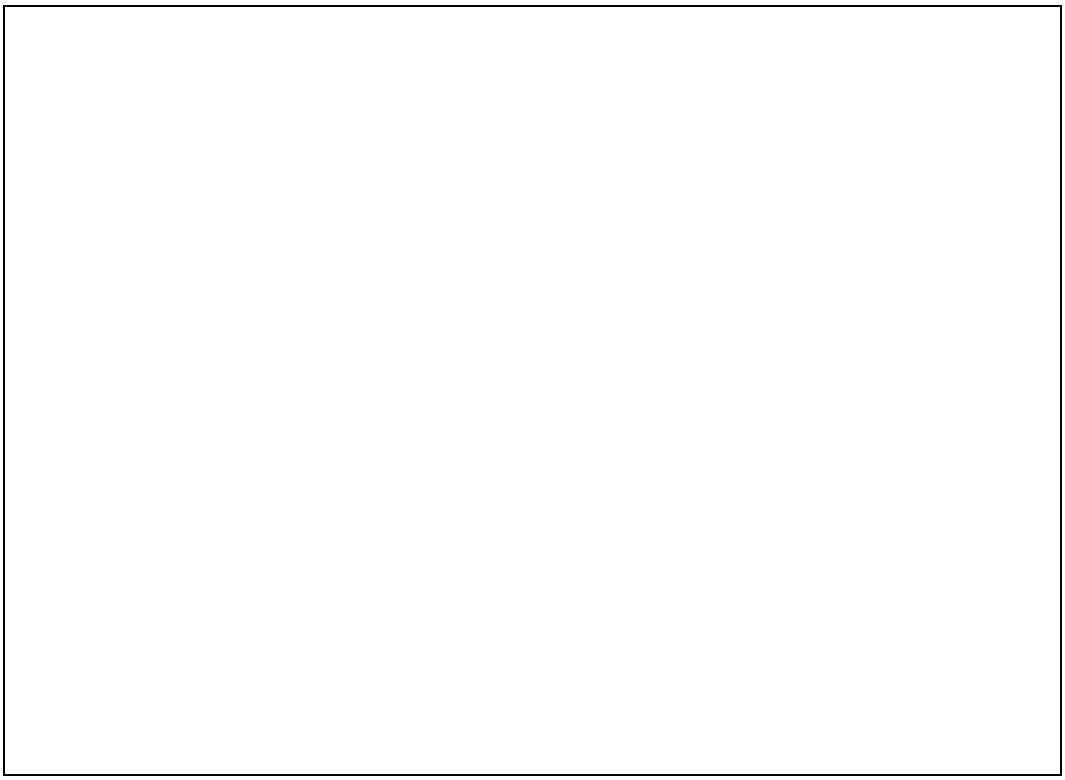

Figure 10: Chamber 1

Chamber 1 (figure **??**) was made from a twenty-centimeter long block of aluminum by boring a hole (eight-centimeter diameter) completely through the center. A second hole of the same diameter was bored into the side of the block till it joined the fist hole at 29^o. The finished chamber looks like a lower case y. The chamber was designed to measure a mirror at 14.5^o and measure the intensity of the source. The distance from the exit slits to the hole in the back of chamber is the same as the total distance from the exit slits to the mirror to the hole in the side of the chamber. These two distances are important because the light coming from the exit slit is diverging. If the two distances are different it will change the relative intensity of the light arriving at the detector.

Absolute reflectivities can be measured using chamber 1 because the intensity of the source and the intensity of the light coming off the mirror can be measured within a short

period of time. The detector is attached to the back of chamber 1 and the intensity of the light is measured. The detector is then moved to the side of chamber 1 and a mirror is put in the center of the beam. The intensity of the light reflected from the mirror is measured. The mirror is removed, and the detector is put on the back again to check the stability of the source. This process is repeated at least twice and may be repeated more times if the source is unstable. The absolute reflectivity can be calculated because the absolute intensity of the source is measured with the same detector that was used to measure the intensity of the mirror.

Chamber 2 (figure **??**) was designed to measure the reflectivity of the curved mirrors for the IMAGE mission. The reflectivity of flat samples could be measured with a special holder that was designed to hold four flat mirrors at the same angle and position as a curved mirror would be in chamber 2. Because of the design it was very easy to measure the reflectivities of the other three mirrors relative to reference mirror of a known reflectivity. As mentioned in section **??** the source is spatially different at 304 and 584 Å. Because of this the samples needed to be realigned when the wavelength was changed. Only one sample needs to be aligned because the mirror holder was machined from one piece of aluminum and the sample positions are fixed. The relative alignment of sample positions has been verified and is not a source of error.

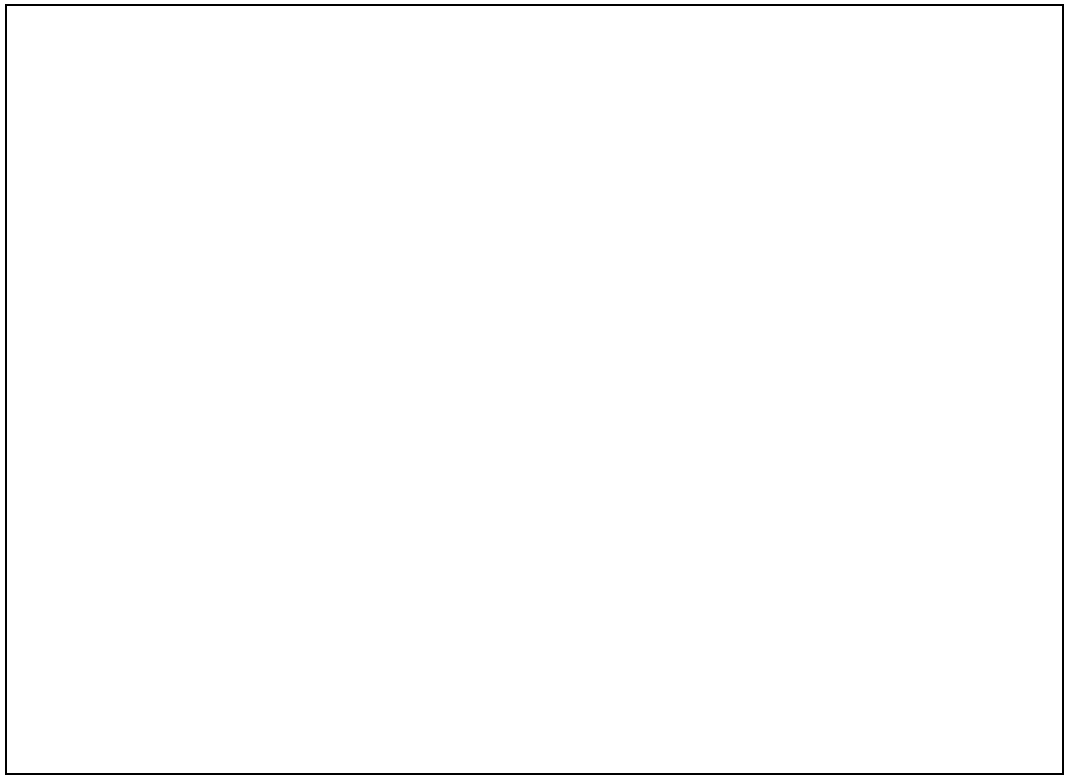

Figure 11: Chamber 2

6.0.4 Detectors

During different phases of research one of two detectors was used to measure the intensity of the light coming from the monochromator and reflecting off the mirrors. A CCD camera

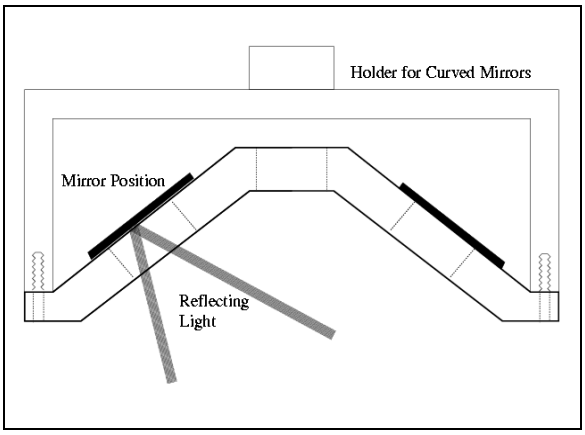

Figure 12: Side View of Mirror Holder

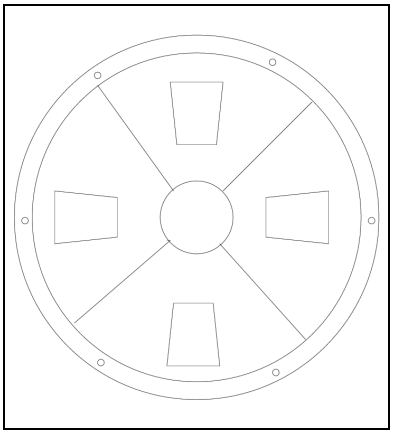

Figure 13: Top View of Mirror Holder

was used to image the spatial variations in the plasma source and to check the alignment of the mirrors in the chambers. A channeltron detector was used to make most of the measurements because it is more sensitive than the CCD camera.

The CCD camera was made by Princeton Instruments and is a back-thinned CCD camera optimized for detection in the EUV. The camera has a 512×512 pixel surface that is 1/2 by 1/2 inches and can produce very detailed images. The benefit of using a CCD camera is the ability to produce an image. This is important because the plasma source discharge is not spatially uniform and it is important to know the shape of the plasma at different wavelengths. There are, however, some disadvantages in using the CCD camera: the camera is not as sensitive as the channeltron, the camera must be cooled to -50 ^{o}C for low noise, and the chip surface is very delicate.

The channeltron detector is a highly sensitive detector that can be run in a variety of modes. The main component of the channeltron is a curved glass tube that is coated with a material that has a low work function. A low work function means that electrons can be ejected from the surface with little energy. There is a large potential difference between the front and back of the glass tube, so when a photon strikes the coating on the glass it ejects several electrons that are accelerated to the other side of the tube. Because these electrons have been accelerated they have more energy and are able to eject more electrons. This process cascades down the tube until thousands of electrons exit the tube. A charge collector records the electron cascade and the collector is reset for the next electron cascade. The channeltron detector has a background count of less than a half count per second. This background is ignored in all measurements because usual measurements average several thousand counts a second.

The channeltron was used for most of the reflectivity measurements because it is more sensitive than the CCD camera. Other benefits of using the channeltron detector are: it is relatively inexpensive, has a low background rate, can detect single photons, is compact, and is very simple to operate. However, it cannot produce an image because it only has a single channel to collect light.

6.1 Data Analysis

Two different methods were used to interpret the data collected at different times. The first method is the less accurate of the two and was the first method developed to collect and analyze reflectivity data. It is a simple method and developed as time went on. The reference mirror is aligned so the greatest amount of counts is reflected from the mirror at a given wavelength. The intensity reflecting from the reference mirror is recorded two or three times to monitor the stability of the plasma lamp. The other samples are then moved into the beam and the intensities of the three samples are recorded two or three times. The intensity reflecting from the reference mirror is measured again, followed by measuring the intensities of the other three mirrors. The reference mirror is measured again to monitor the long-term stability. This method records the reflected intensity several times and records some of the variations in the source, but does not give a measure of the long-term variations of the mirror.

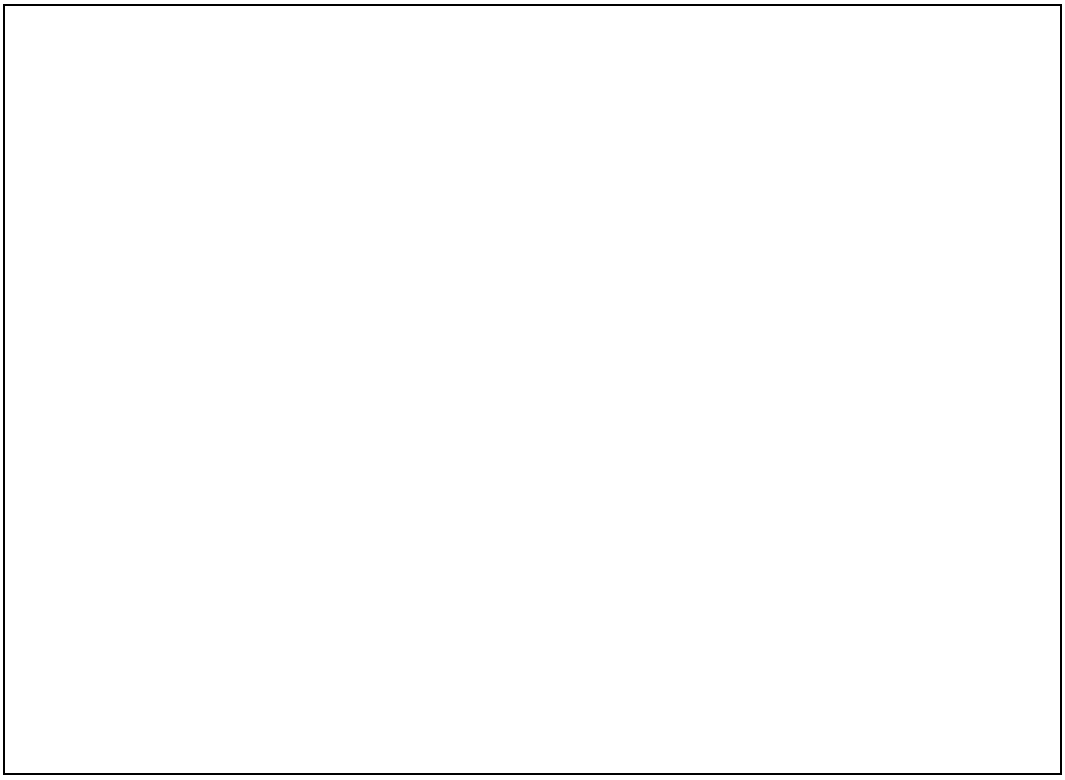

Figure 14: Raw Data at 304 Å

The second method was developed in January of 1999 and used a computer to record the time variations in the source. The channeltron detector uses a program written at BYU that can take and record a continuous stream of data. The reference mirror is first aligned to give the highest reflected intensity, the other samples are aligned in the same way to assure the relative alignment of the samples is the same. The program is started and the channeltron begins to take data at a regular time interval. The exposure time depended on the intensity of the source, and is adjusted so the counts were at least in the several thousands of counts per exposure. All the samples are measured without turning off the detector. The change in samples is obvious when looking at the data because there is a

sharp dip in the number of counts that rises again very rapidly. If the mirrors have different reflectivity the difference is also notable. The same cycle, as used in the first method, is used to measure all the samples. Because the computer is continuously taking data at a set time interval, the long-term trends in the intensity of the source are easily distinguished. The amount of data gathered, using the second method, is significantly greater than the amount of data gathered using the first method.

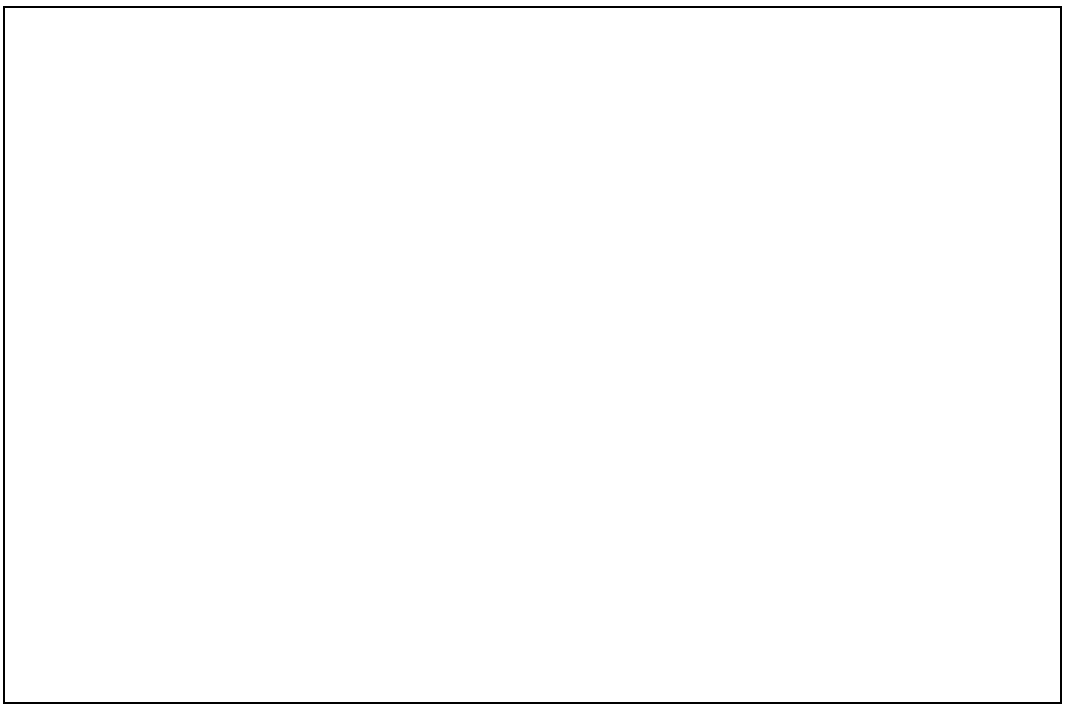

Figure 15: Parsed Data at 304 Å

The data from the saved file is then entered into a spreadsheet and parsed into separate bins that corresponded to each mirror. The corresponding times when the mirrors were changed and when the signal was stabilizing are removed. An example of removing data which comes from these times can be seen by comparing graphs **??** and **??**. After the data is parsed the intensity of the light reflected from each of the mirrors is fit to a line using Quattro Pro's Regression Tool. The output includes the standard deviation of the offset b (see equation **??**). This deviation was used to compute the propagated deviation with the deviation of the reference mirror. The deviation in the slopes of the lines was not used except to calculate the deviation of the source intensity. The slopes of the measured intensities from the samples are different on a linear plot, because the slope depends on the reflectivity of the mirror coating (see figure **??**). The fitted data is also graphed on a log plot to check the validity of the data. If the difference in the slopes is only dependent on the reflectivity the slopes of the lines on a log scale will be the same (see figure **??**). This happens because the function of a line is $y = mx + b$ and when a line is graphed on a log plot the following happens.

$$ln(y) = ln(mx) + ln(b) \qquad \text{becomes} \qquad ln(y) = ln(m) + ln(x) + ln(b) \tag{19}$$

On a linear plot the slope was multiplied by the dependent variable and was dependent on the reflectivity of the mirror. On a log plot the slope and the dependent variable are

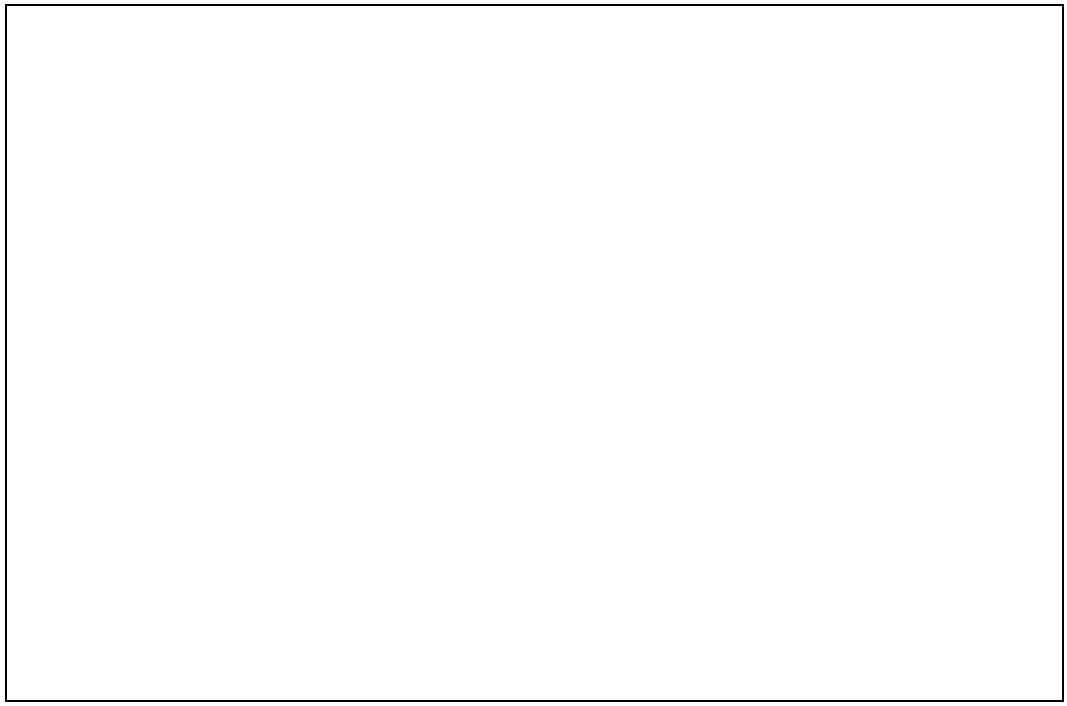

Figure 16: Linear Fit of Data at 304 Å

separate, so the graphed lines will have the same slope if the data is valid. Any data that did not meet this criteria was discarded.

Once the data has been fit to a line, the verified differences in the slopes only depends on the differences in the reflectivity of the mirror and the reflectivity of the mirrors is calculated. Only the intensity of the light coming from the exit slits is calculated from the fitted data by

$$I_o = I_{Ref} \frac{100\%}{R_{Ref}} \tag{20}$$

where I_{Ref} is the calculated intensity reflected from the reference mirror and R_{Ref} is the reflectivity of the reference mirror. A 200 Å monolayer of molybdenum was used as the reference mirror because molybdenum will form a native oxide in a few days that is 15–20 Å thick and should then be stable for a long period of time. A single layer of molybdenum will also reflect three to five percent at 304 Å and will reflect 10–16 percent at 584 Å.

The reflectivities of the mirror coatings being measured were calculated by dividing the measured intensity reflected from a mirror coating by the calculated intensity of the light coming from the exit slits. Because the intensity could be calculated at any time the calculated reflectivities using method two included the time variations in the plasma lamp.

The raw data taken from the mirrors gave multiple numbers for each mirror. The differences in these numbers come from multiple sources. There are normal statistical variations because the detectors count a finite number of photons in a finite time. These variations should be roughly Gausian. There are variations in the deposition of the multilayer mirror coatings, making each coating be slightly different. There are variations in the measurement of the reflectivities. The plasma lamp is known to be unstable and each mirror may be aligned slightly different. These variations make it impossible to determine the exact

reflectivity of a multilayer mirror coating, but it is possible to determine the reflectivity within a statistical margin of error. By understanding how these statistical methods work it is possible make measurements with small deviations from the average value.

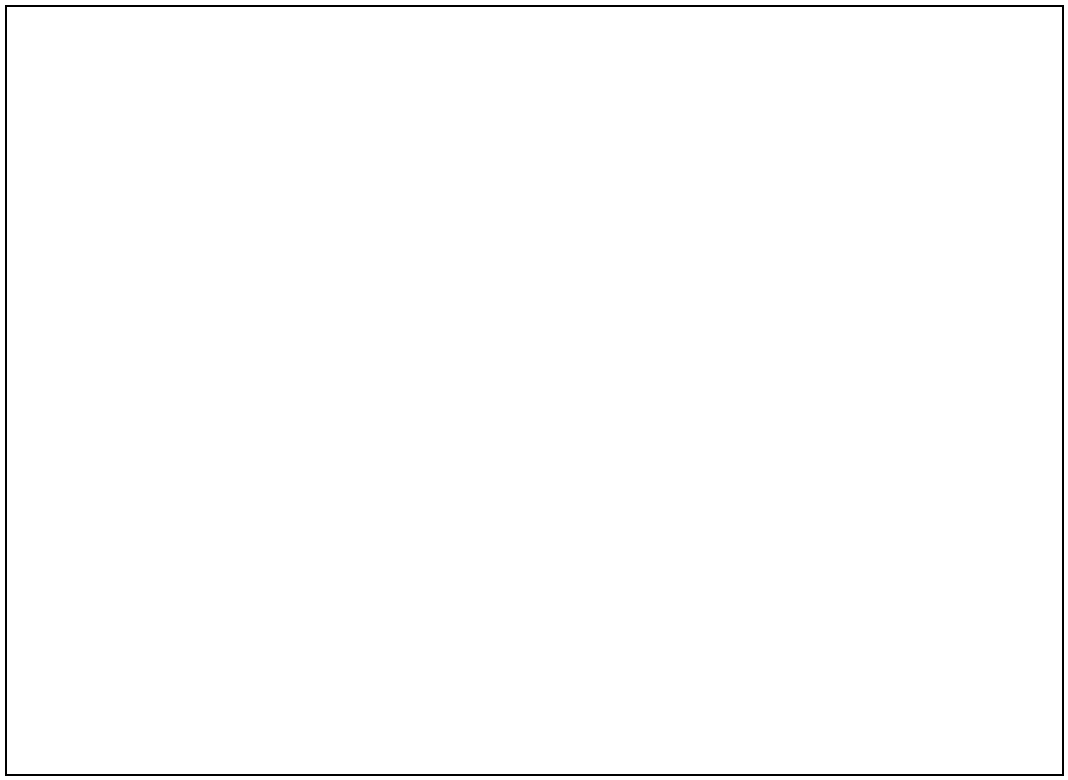

Figure 17: Log Plot of Fit Data at 304 Å

6.1.1 Statistical Methods

There are two types of error: statistical and experimental [**?**]. Statistical error comes from fluctuations that are inherent in making any measurement. These errors can be reduced by making more measurements which will narrow the error bars around the real value. Experimental errors are caused by faulty equipment, procedures, or the researcher. This type of error should be discovered and changed so the error is mostly statistical. The majority of the error in this thesis is experimental error because of the limitations inherent in the measurement chambers. The statistical error is a small factor in the error in this thesis. The statistical error is reduced by counting till the minimum number of counts in a measurement is greater than one thousand, and many times it is greater than one thousand.

Several reflectivity measurements will map to a single point with an error bar by using very simple statistical methods. The sample mean is defined as

$$\bar{x} = \frac{\sum^{N} R_n}{N} \tag{21}$$

The sample variance is the average a single measurement deviates from the sample mean. It is defined as

$$s^2 = \frac{\sum^{N} (x_i - \bar{x})^2}{N - 1} \tag{22}$$

It can be seen that the larger N is, the smaller the standard deviation will be. If the measurements are fairly consistent it is possible to reduce the standard deviation by making the measurement many times. The numerator is divided by $N - 1$ because there are a finite number of measurements. At least one measurement is devoted to determining the sample mean so it can not be included in the calculation of the sample variance.

The sample standard deviation is defined to be

$$s = \sqrt{s^2} \tag{23}$$

The sources of error in calculating the optical constants are: source instability, statistical fluctuations in counting, error in the calculation of the reflectivity of the reference mirror, and variations between different measurements.

Because there are several sources of measurable error they must be combined to a single error that represents all the sources of error. The method to calculate the combined error from multiple sources is similar to finding the distance between two points in multiple dimensions. Combined error from multiple sources is defined

$$s = \sqrt{\sum^{N} \frac{s_i^2}{\bar{x}}} \tag{24}$$

and is known as the propagation of errors.

6.1.2 Data 304 and 584 Å

Only multilayers with a Γ of 0.7 ± 0.03 were used in the fitting. All the mirrors were measured multiple times, but some measurements are more reliable than others and were weighted. The graphs of all the data points were made using Corel Quattro Pro. The error bars are calculated by the methods explained in the Statistical Methods section. The graphs of the compiled data were plotted using IMD 4.1. Two sets of data were used at 304 and 584 Å to

determine the shift in the optical constants of amorphous silicon and uranium. One set used multilayer mirror coatings that were capped with a thin layer of uranium that was allowed to oxidize, and another set with an amorphous silicon capping layer that was also allowed to oxidize. Experience show the uranium layer oxidizes completely, but the silicon layer only oxidizes 10 to 20 Å. There is error inherent in both sets, but there are less multilayers with an amorphous silicon cap because the uranium cap suited the design of the IMAGE mission. There are many multilayers with a uranium cap, but the optical constants of uranium oxide are not known and the capping layer is not consistent over the whole range. By fitting these two cases separately the magnitude and direction of the change in the optical constants can be determined.

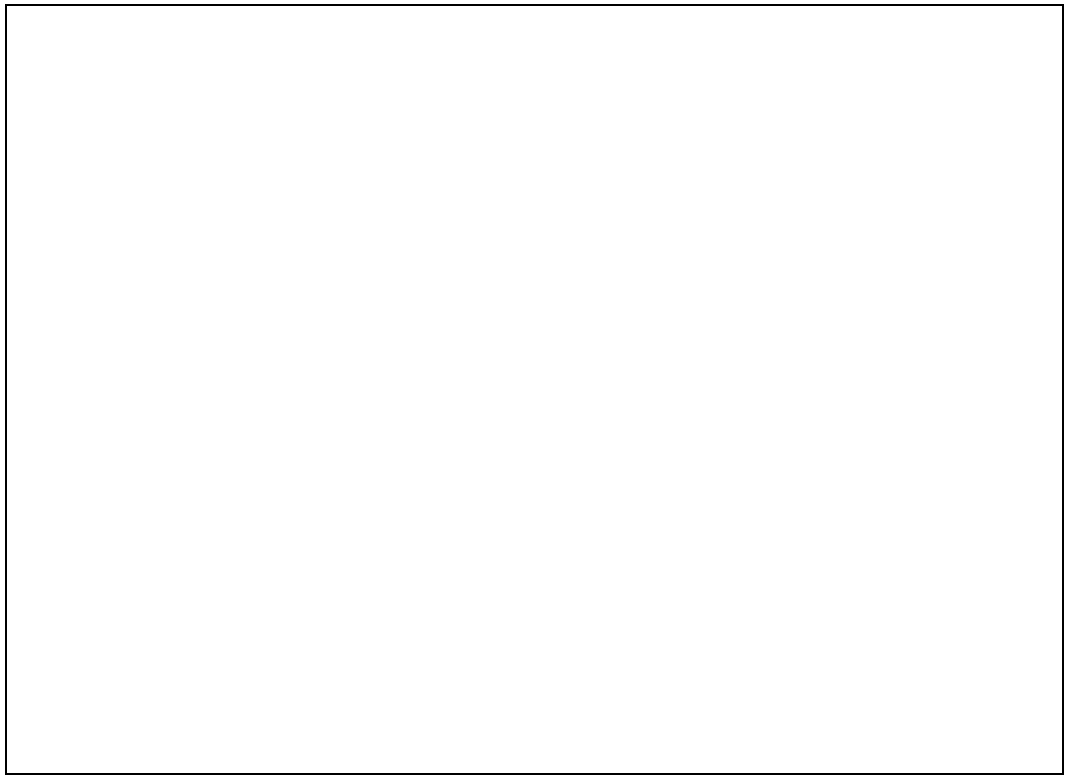

Figure 18: Scatter Plot of all Multilayer mirrors with no overcoat at 304 Å

In the process of designing multilayer mirror coating for the IMAGE mission it was found that putting a thin layer of uranium on the top of the multilayer and allowing it to oxidize would increase the reflectivity of the mirror and protect the multilayer from further oxidation. There is some ambiguity to the shape of the peak when only multilayers with no overcoat are considered. By comparing figures **??** and **??** it is possible to better understand the shape of figure **??**. The multilayer mirrors with an overcoat reflect one to two percent more than multilayer mirrors without an overcoat and the peak in figure **??** appears to be more narrow than the peak in figure **??**. These effects are important in and of themselves but will not be discussed in this thesis.

It can be seen on figure **??** that the reflectivity measurements of U8Si128, U8Si127, and U8Si109 vary significantly between different measurements. The cause of such large variations has not been determined conclusively, but it seems likely that the reflectivity

near the top of the peak is very sensitive to some unknown parameter. The measurements of U8Si128 and U8Si127 were made without the sample being moved so it is assumed that the beam of light was striking nearly the same place on the sample every time. It can be noted that U8Si126 varied little while being measured at the same time as U8Si128, U8Si127. Again it is helpful to compare figures **??** and **??** and notice the variations at the peak of the curve. The low values of U8Si109 were ignored when calculating the average value of the measurements and the variation, because of the complexity of calculating a weighted fit.

As mentioned above the presence of an oxidized uranium layer of the correct thickness increased the reflectivity at 304 Å. This oxide layer also affects 584 Å but the effect is more pronounced at 584 Å. A layer of SiO_2 will also change the reflectivity of a multilayer but the oxidation of the top layer of amorphous silicon takes several days to reach a quasi equilibrium, as compared to uranium that oxidizes in a few minutes. The oxidation of the top layer affects the reflectivity at 304 Å less than it affects the reflectivity at 584 Å. This means that as a multilayer mirror terminated in amorphous silicon ages in time the reflectivity at 584 Å will have a larger relative change than at 304 Å. The overall effect is seen by comparing the calculated reflectivity of a varying SiO_2 layer at 304 and 584 Å (see figures **??** and **??**).

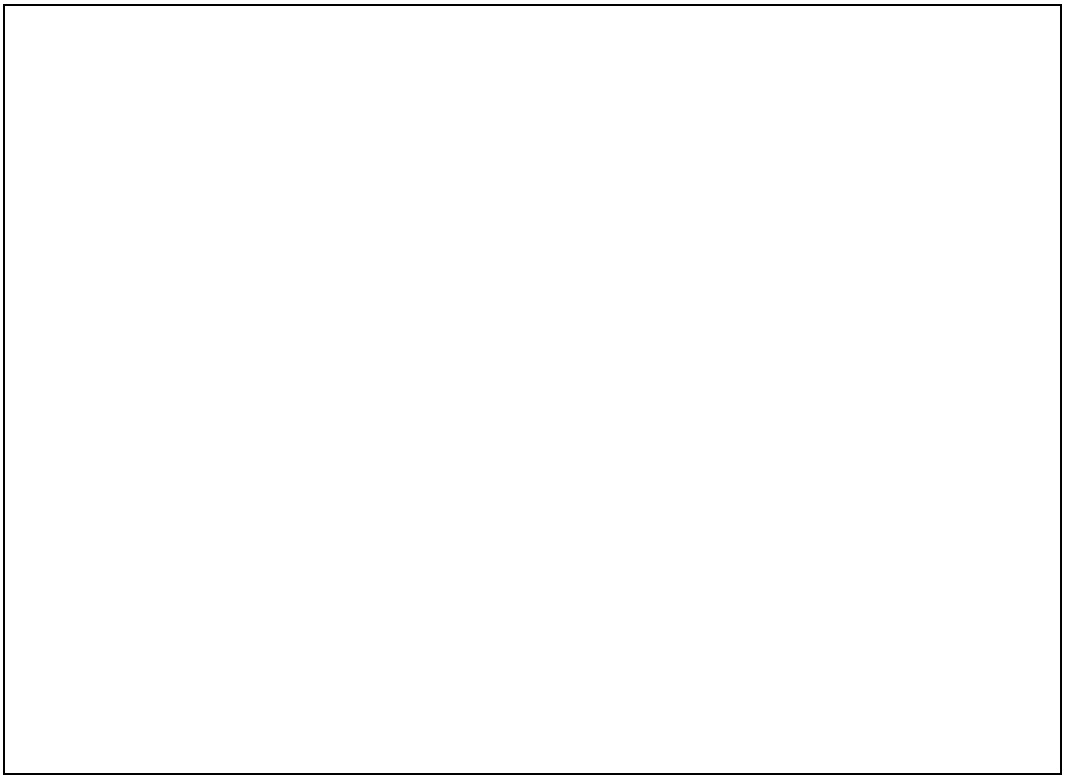

Figure 19: Scatter Plot of all Multilayer mirrors with uranium oxide overcoat at 304 Å

There is a great deal of scatter in the measurements of multilayers terminated in amorphous silicon at 584 Å, but by comparing measurements made on multilayer mirrors with an uranium oxide coating and the reflectivity calculated using preexisting optical constants it is possible to eliminate some data points that are nonphysical. The large variation may come from aging, mismeasurement, or mischaracterization. The reason for the variations are not known at this time but by comparing the measurements of multilayers terminated in uranium, the shape of the curve can be approximated.

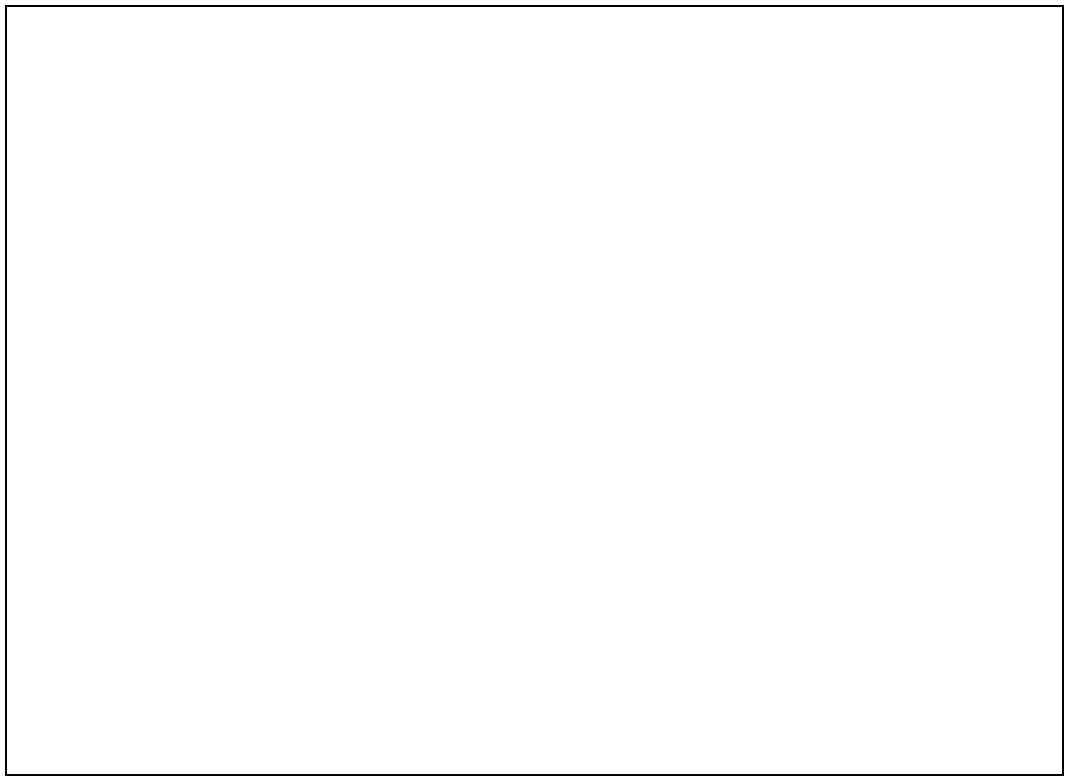

Figure 20: Scatter Plot of all Multilayer mirrors with no overcoat at 304 Å

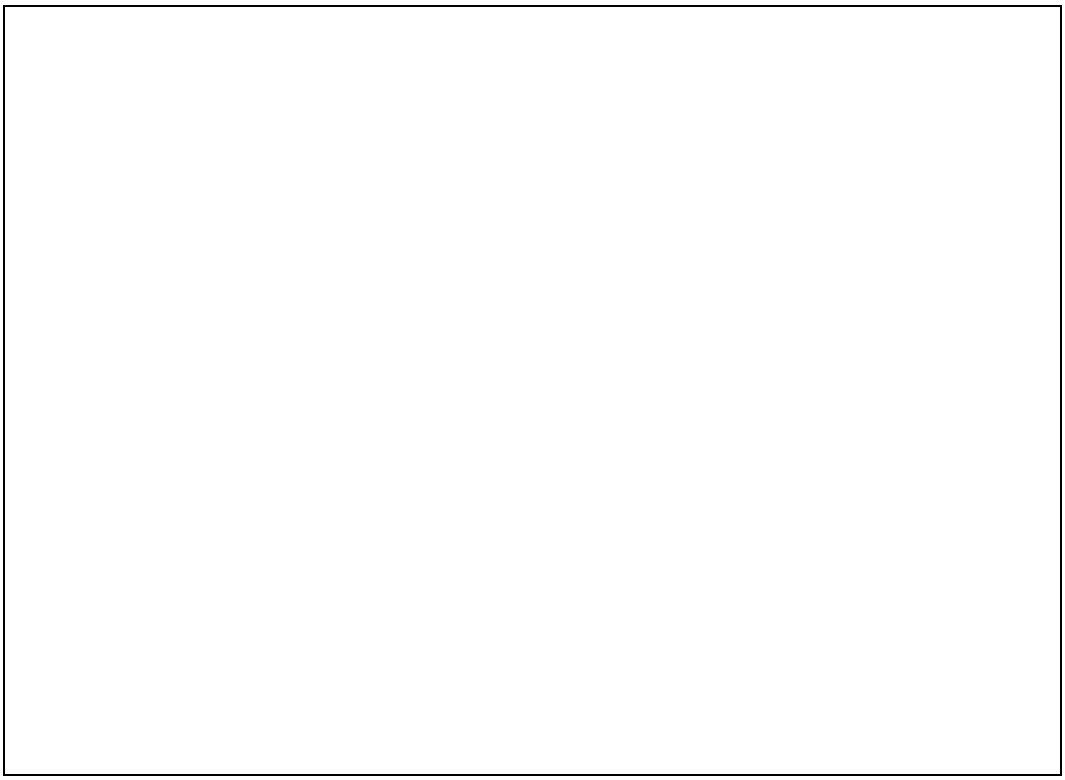

Figure 21: Scatter Plot of all Multilayer mirrors with uranium oxide overcoat at 304 Å

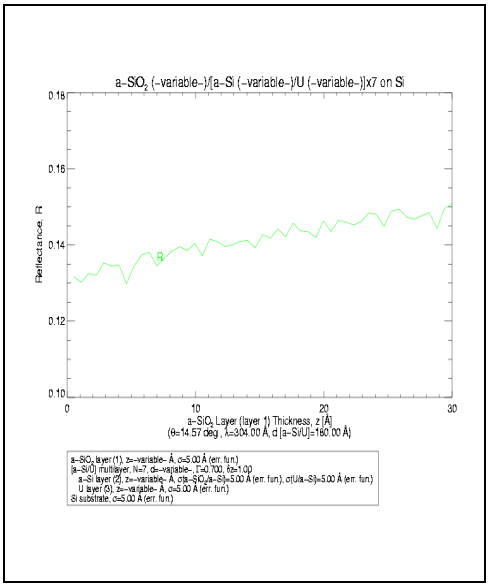

Figure 22: Reflectivity at 304 Å as a function of SiO_2 thickness

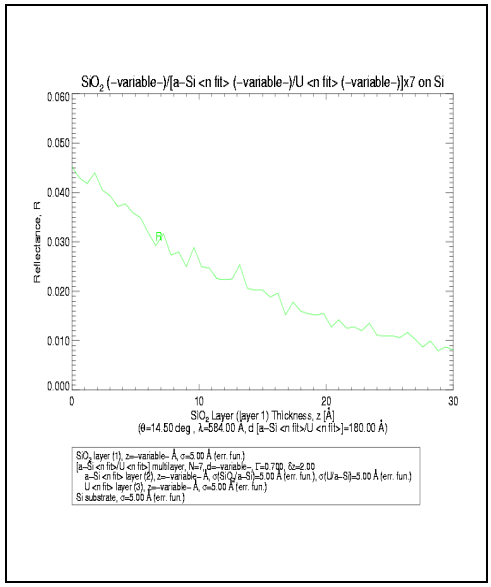

Figure 23: Reflectivity at 584 Å as a function of SiO_2 thickness

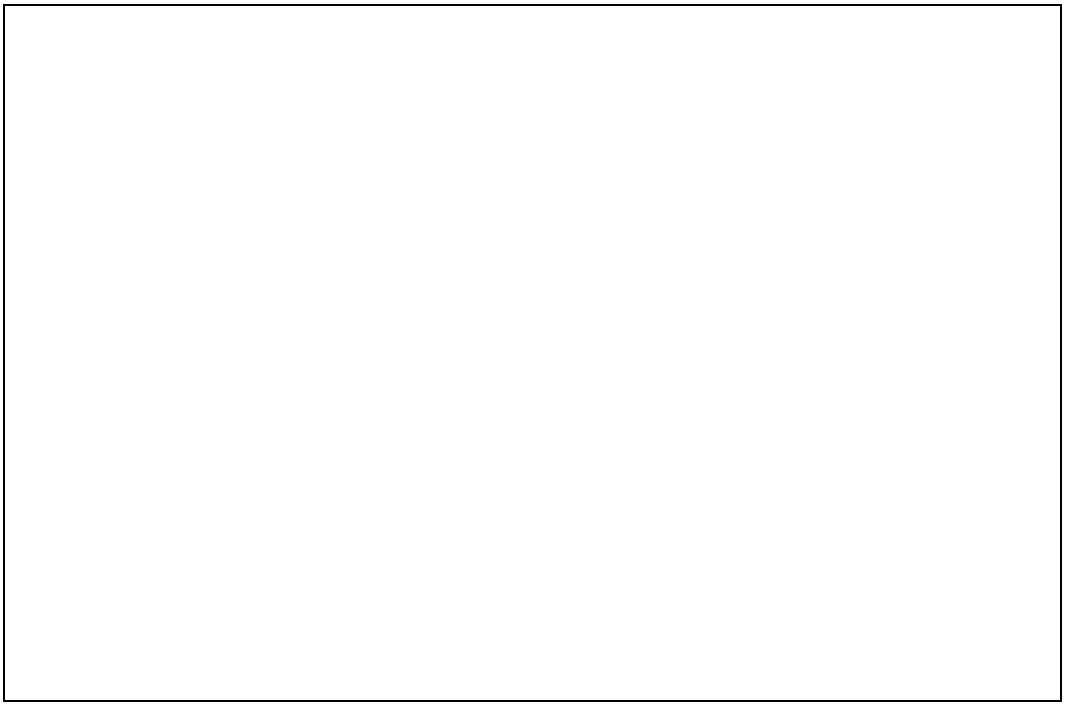

Figure 24: Scatter Plot of all Multilayer mirrors with no overcoat at 584 Å

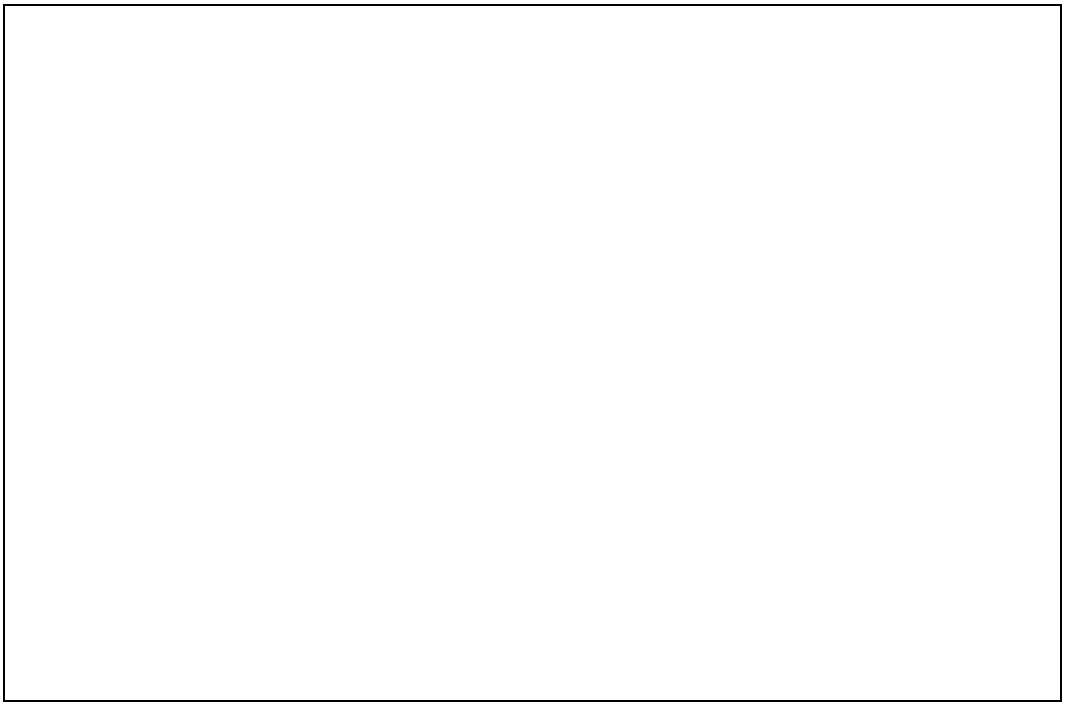

Figure 25: Scatter Plot of all Multilayer mirrors with uranium oxide overcoat at 584 Å

7 Calculated R is different than Measured R

There are several indications that the optical constants are not well known in the EUV. The optical constants of a-Si from peer reviewed literature are not consistent with optical constants calculated from the atomic scattering factor of c-Si [**?**]. In addition, peer reviewed data sets do not make a smooth boundary when merged together.

The measured reflectance from multilayer mirror coatings and the reflectance calculated from preexisting optical constants are different at 304 and 584 Å. All the mirror coatings were made from uranium and amorphous silicon with Γ 0.7 ± 0.03 over a range of layer thickness from 150–270 Å. All the mirrors were measured at 14.5^o from normal.

7.1 304 Å

At 304 Å the measured reflectivity peak position was shifted 5 Å towards a higher layer thickness than calculated. The difference is not as pronounced as it is a lower energies, but is significant. This may show the optical constants are not well known at 304 Å. It also shows that at 41 eV there is still the possibility of chemical effects changing optical constants. It is not certain these changes are due to measurement uncertainty or chemical effects.

In figures **??** and **??** it can be seen the reflectivity is lower and the peaks are shifted towards a thicker layer period. When the optical constants are fit using the multilayers with a uranium cap the n's of uranium and amorphous silicon are both closer to unity, so the wavelength of light will be longer in the uranium and amorphous silicon. That may be one reason the peak is shifted to a higher layer thickness.

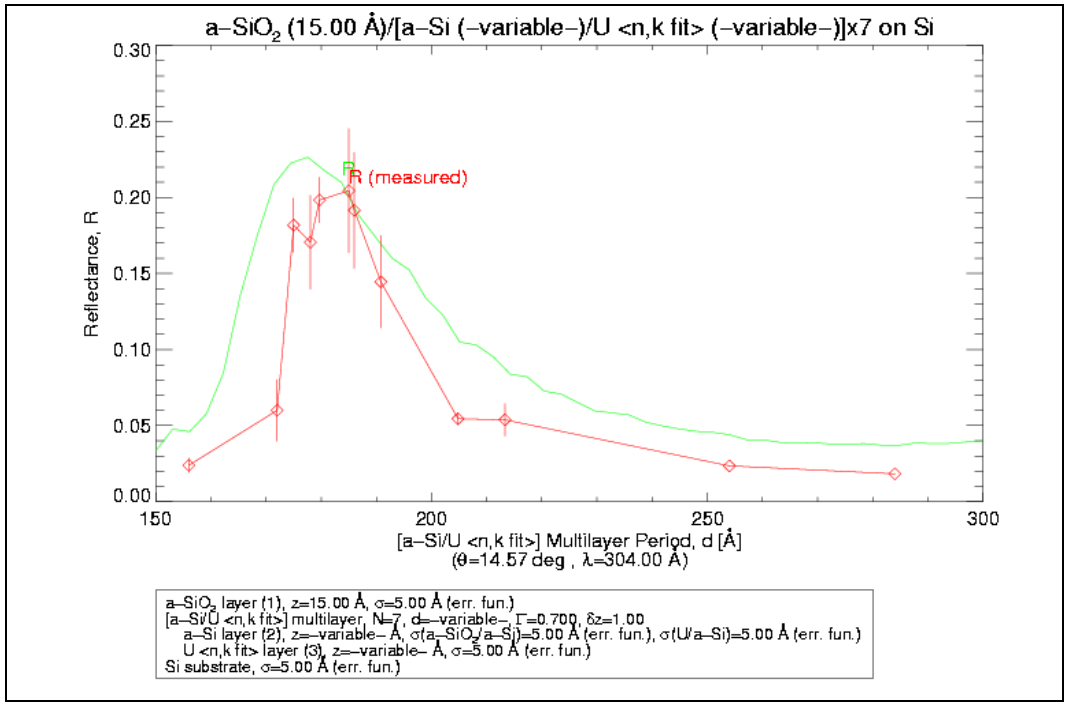

Figure 26: Measured and Calculated Reflectivities with amorphous silicon cap at 304 Å

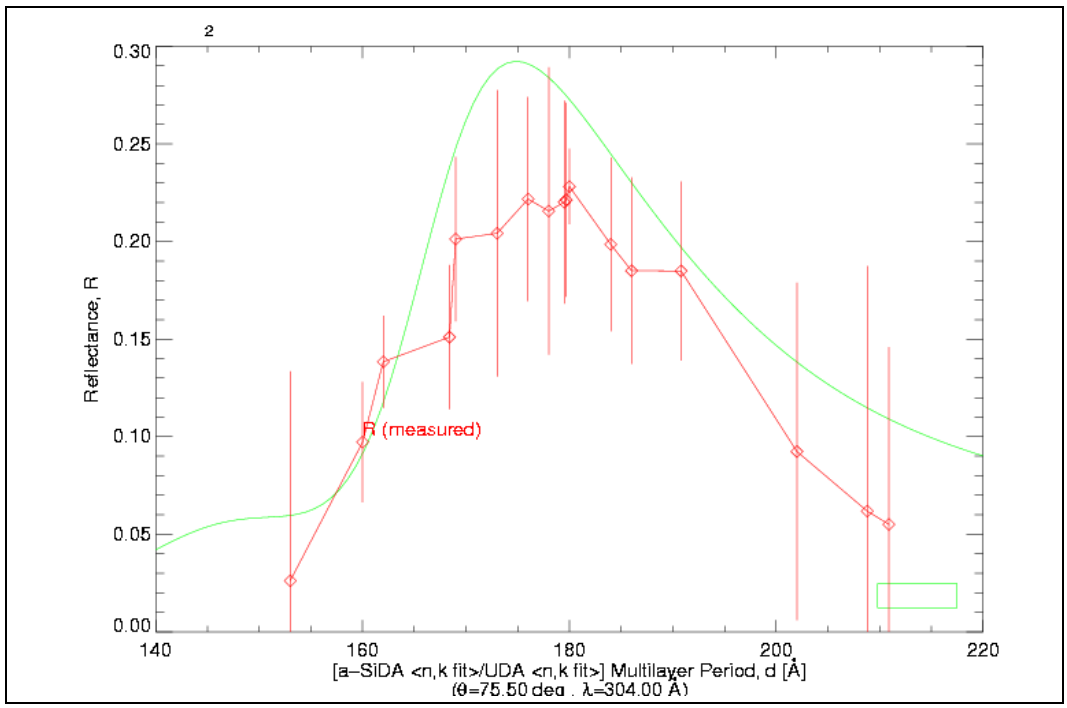

Figure 27: Measured and Calculated Reflectivities with uranium oxide cap at 304 Å

7.2 584 Å

At 584 Å the shape of the reflectivity versus period curve can be approximated by a straight line. This is expected because the multilayers were designed to have a broad minimum around 584 Å, however the reflectivity is very low compared to the calculated reflectivity. This low reflectance is much lower than can be expected if roughness is the only factor affecting the reflectivity, because longer wavelength light (584 Å) is scattered less by roughness than shorter wavelength light (304 Å). If roughness was more than approximated it would have lowered the reflectivity at 304 Å more than at 584 Å. It can be seen by comparing figures **??** and **??** the uranium oxide cap lowers the reflectance at 584 Å. Even though the data for multilayers capped with amorphous silicon is not as smooth as the multilayers capped with uranium oxide, the slope and reflectance of the measured data does not agree with calculated values. Multilayers capped with uranium oxide are between 1/2 to 1/3 less reflecting that would be expected. This effect may be due to the presence of the uranium oxide layer, rather than a deviation from published the optical constants of amorphous silicon and uranium.

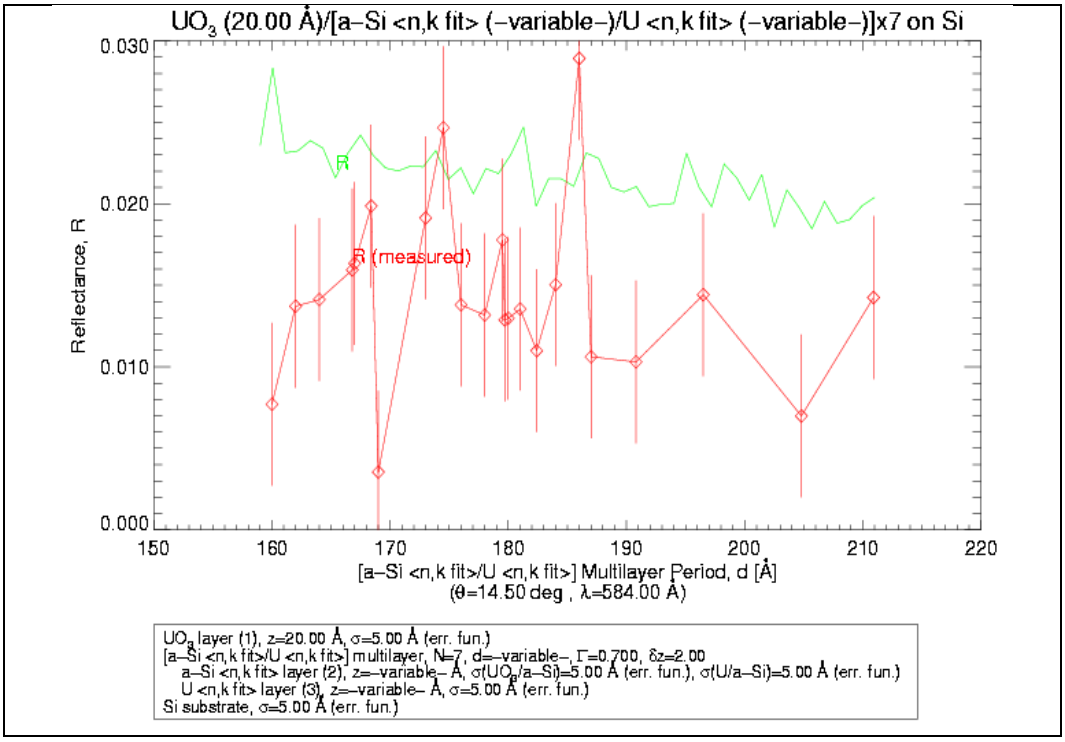

Figure 28: Measured and Calculated Reflectivities with uranium oxide cap at 584 Å

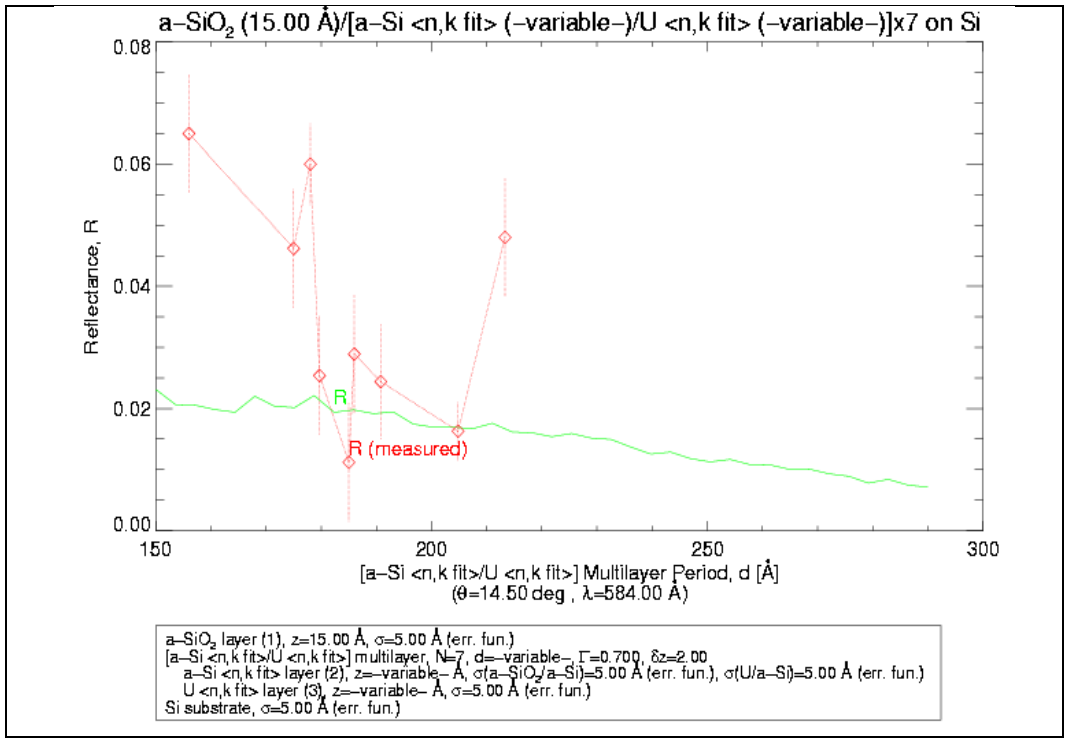

Figure 29: Measured and Calculated Reflectivities with amorphous silicon cap at 584 Å

The relative difference in the multilayer reflectance at 584 Å was more pronounced than at 304 Å. This was expected because 584 Å is a lower energy then 304 Å, and would be more affected by the chemical bonding of the materials in a multilayer. It also shows the current understanding of optical constants in the EUV is deficient. Chemical effects may be changing the optical properties of the materials in the multilayer, but the optical constants of compounds are not as well known at 584 Å as they are at 304 Å. It may be a combination of chemical effects and uncertainty in the optical constants. If bonding energetics are the cause of the difference will most likely be a weak interaction between the chemical bonds and the inner structure of the atom.

8 Calculated Optical Constants

8.1 Using IMD

First a model of the multilayer mirror must be provided for IMD. The measured data is then read into IMD from an ASCII text file that includes layer thickness, reflectivity, and statistical error. The number of fitting parameters that can be chosen depends on the number of data points. More fitting parameters can be used if there are more data points, but care must be taken to avoid fitting a physical feature with a nonphysical parameter. IMD will also calculate the confidence interval over a user-defined grid space to determine the goodness of the fit.

Two versions of IMD were used in the fitting and calculation of confidence integrals. IMD 4.0 had many bugs and was more limited in fitting optical constants to measured data, but it fit the data well and produced confidence integrals that appear to be reliable. Version 4.1 of IMD has many more fitting options, but never converged on the value of various optical constants. Even when the uranium capped data was fit at 584 Å, IMD 4.1 did not converge. This may be happening because there is a lack of data, but IMD 4.1 seems to fit differently than IMD 4.0.

8.1.1 Fitting and Confidence Integrals

The measured reflectivities are used to calculate the optical constants of uranium and amorphous silicon by fitting a model of the multilayer to the measured data points. IMD was used to fit the optical constants to the measured data. IMD uses CUREFIT and the Marquardt method of non-linear least squares fitting [**?**]. The data for the uranium capped multilayers was well fit by IMD. The data for the amorphous silicon capped multilayers was not fit well by IMD. This data was fit by hand using IMD. The real part of the index of refraction was primarily fit, because a four dimensional space of the real and imaginary parts of the optical constants of uranium and amorphous silicon is near impossible to fit by hand. By an iterative process the thickness of the SiO_2 was determined to be 11 Å, and it was assumed there is 5 Å surface and interfacial roughness [**?**].

The uranium capped data were fit with IMD 4.0 several months previous to the fitting of the amorphous silicon capped data with IMD 4.1. The uranium capped data were analyzed using the first data analysis method, and the error calculation was not as rigorous as the error calculation for the amorphous silicon data. Even though the analysis of the uranium capped data is less rigorous, the larger data set makes the fitting of the uranium capped data more reliable than the fitting of the amorphous silicon data.

To calculate the reliability of the fit, a confidence integral is calculated for the optical constants of uranium and amorphous silicon. The confidence integrals were calculated using

IMD over a user defined parameter space. The resolution and the freedom are determined by assuming the reliability of the preexisting optical constants. The optical constants at 304 Å are assumed to be more reliable than the optical constants at 584 Å. The goodness of the fit is represented by χ^2 and the closer χ^2 is to unity, the more reliable the fit.

8.2 304 Å

The confidence integral calculated for the uranium capped data shows the fit in n is better than the fit for k. The calculated χ^2 varies from one to ten so the fit is good. The confidence integral for multilayers capped with amorphous silicon shows the fit is minimized but χ^2 several thousand. This means the fit is not reliable even though the fit is minimized and fits the data well. However it seems fitting and calculating confidence integrals in IMD 4.1 is different than IMD 4.0. IMD 4.0 was used to fit and calculate the confidence integrals for multilayers with a uranium cap.

The optical constants at 304 Å of a-Si calculated from multilayers terminated with uranium oxide are $k = 0.037 \pm 0.015$, a positive 400% shift and $n = 0.961 \pm 0.025$, a positive 3.5% shift, and the optical constants of U are $k = 0.67$, a negative 380% shift, and $n = 0.69$, a positive 2.4% shift. The refractive index of a-Si at 304 Å calculated from multilayers terminated with amorphous silicon is $n = 0.939$, a negative 1% shift and the refractive index of U is $n = 0.705$ a positive 4% shift. The refractive index of amorphous silicon does not seem to change significantly, but the absorptive constant of amorphous silicon changed drastically. The refractive index of uranium increase in both calculations and the confidence integral of calculations made on multilayers terminated with uranium oxide shows this fit is good, but the absorptive constant of uranium changed drastically and is not a well determined as the refractive index.

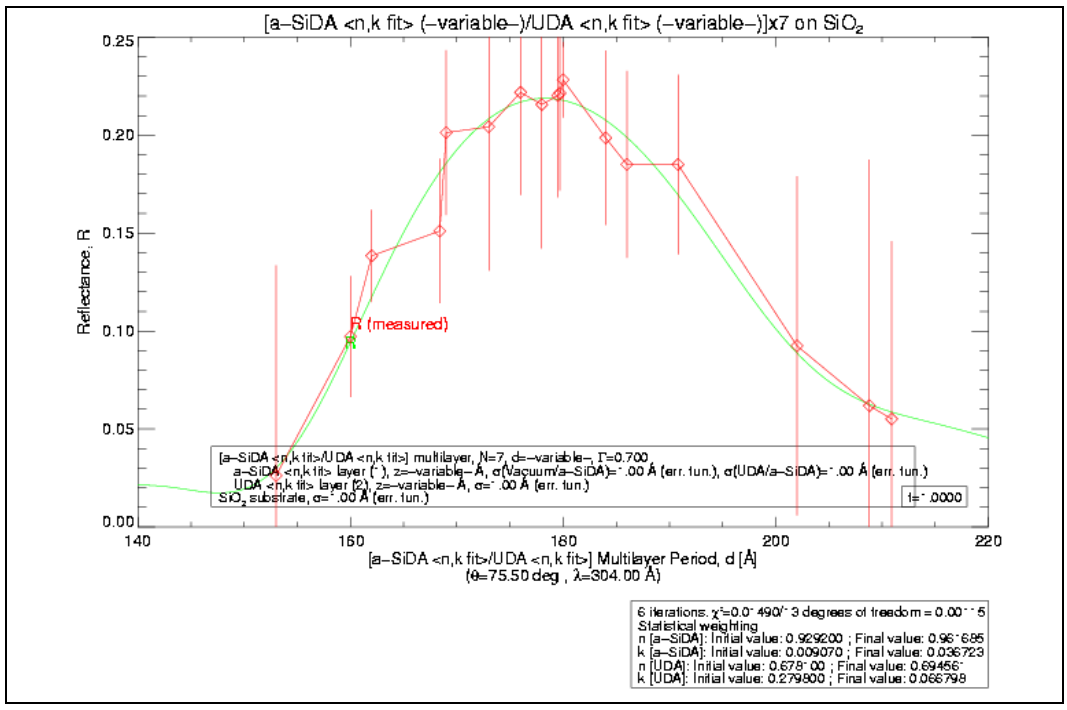

Figure 30: Fit n for a-Si and U at 304 Åwith uranium oxide cap

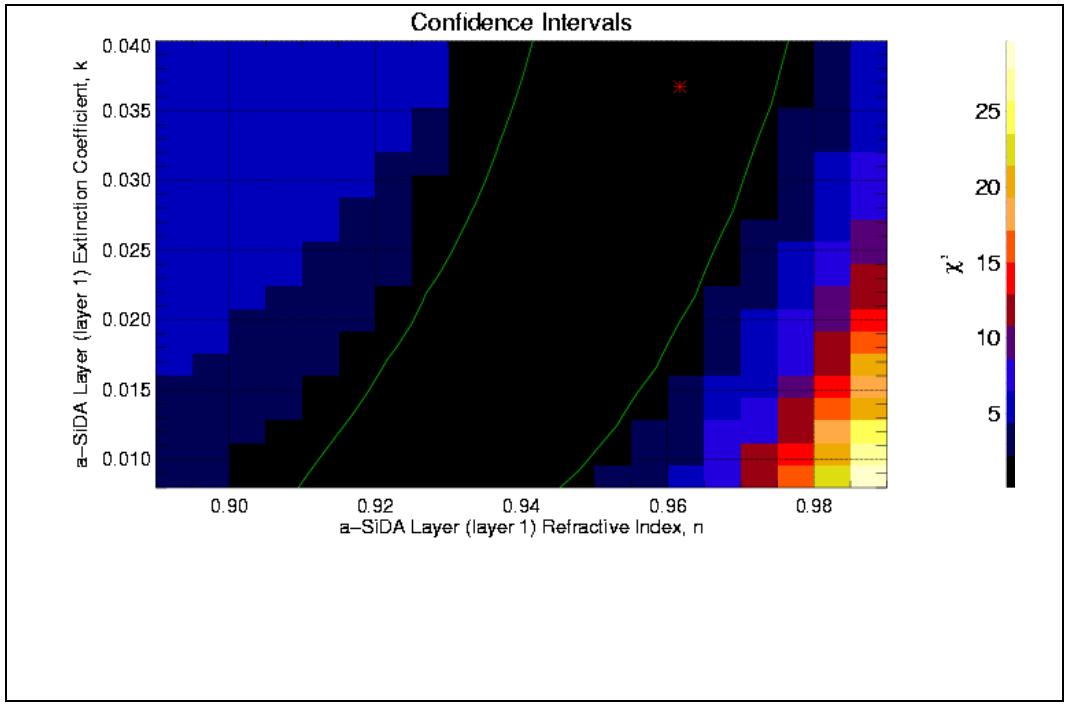

Figure 31: Confidence Integral of n for a-Si and U at 304 Å with uranium oxide cap

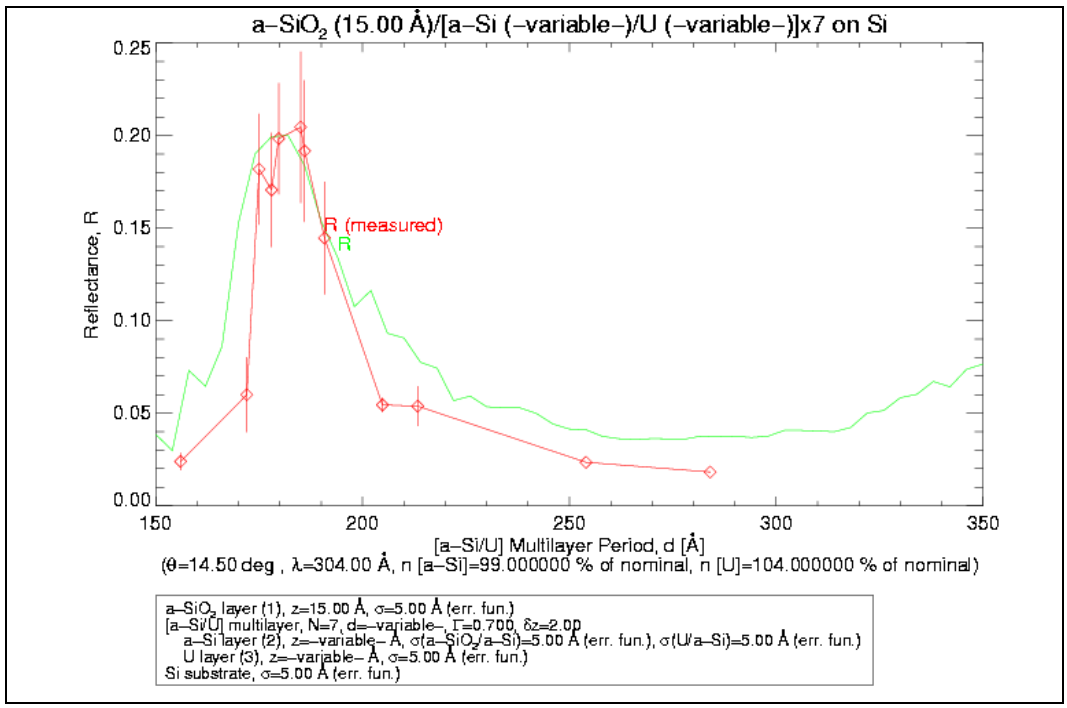

Figure 32: Fit n for a-Si and U at 304 Å with amorphous silicon cap

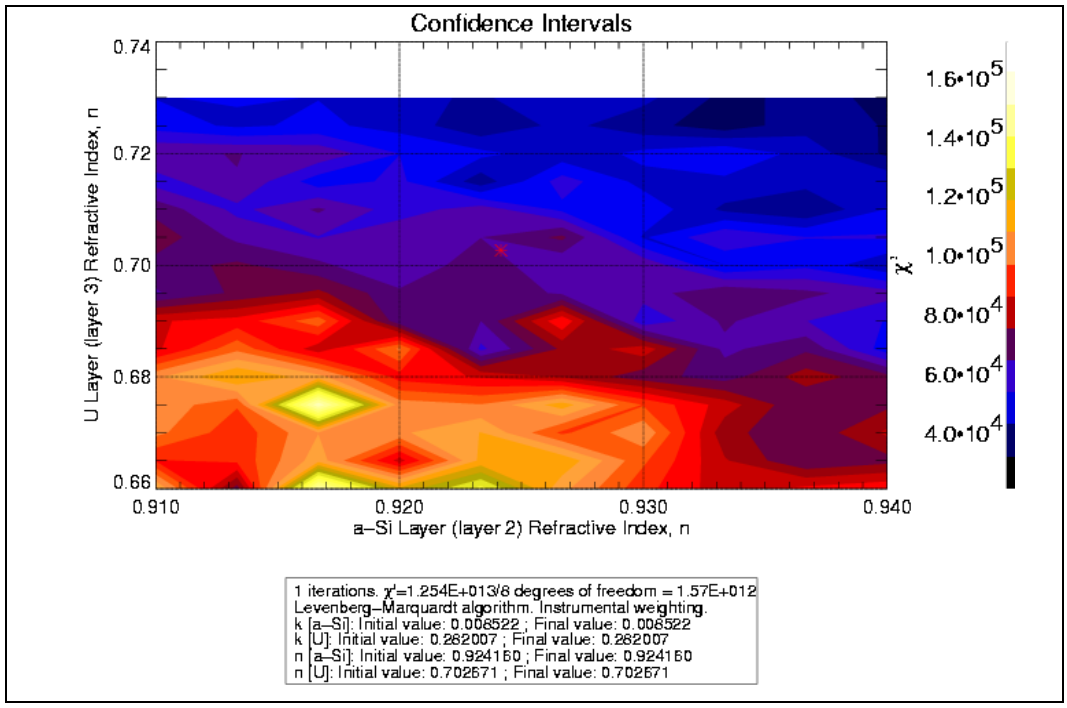

Figure 33: Confidence Integral of n for a-Si and U at 304 Å with amorphous silicon cap

8.3 584 Å

Fitting the reflectance data to optical constants at 584 Å was not as successful as it was at 304 Å. Both sets of data were fit by hand. The confidence integral had a minimum χ^2 of 40. It can also be seen that the value of the confidence integral depended most on the index of refraction of uranium. As mentioned in the introduction many values at 584 Å were extrapolated. Silicon is a material that has been studied more than many other materials. In hindsight it is understandable that the optical constants of silicon would be known better.

The refractive index at 584 Å of a-Si calculated from multilayers terminated with amorphous silicon is $n = 0.806$, a positive 2% shift, and the refractive index of U is $n = 0.55$, a negative 6.8% shift. The refractive index at 584 Å of U calculated from multilayers terminated with uranium oxide is $n = 0.49$, a negative 17% shift. The refractive index of amorphous silicon changed 7% when calculated with multilayers terminated with amorphous silicon, but the refractive index of amorphous silicon changed 17% when calculated using multilayers terminated with uranium oxide. The difference between the two calculated values of the refractive index may show the unique properties of uranium oxide cap at 584 Å. The refractive index calculated from multilayers terminated with uranium shifts the refractive index of uranium lower than calculated with multilayers terminated with amorphous silicon, even though the magnitude of the shifts are different the direction is the same. The difference in the magnitudes of the shifts may show the importance of the oxide layer at 584 Å.

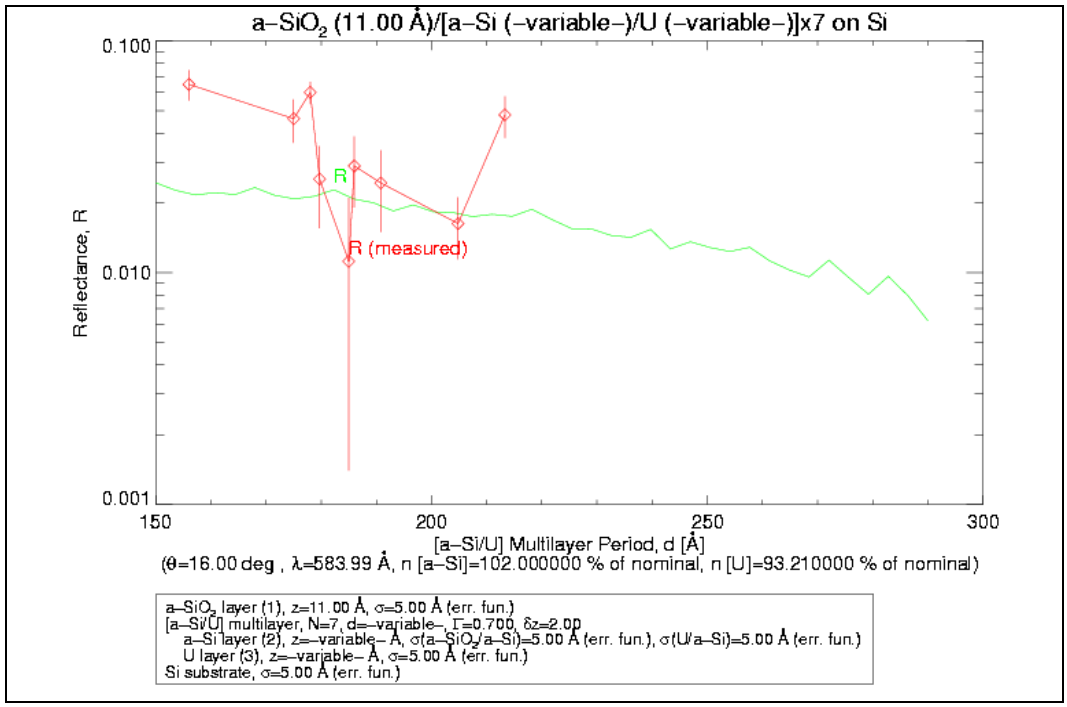

Figure 34: Fit n of a-Si and U at 584 Å with amorphous silicon cap

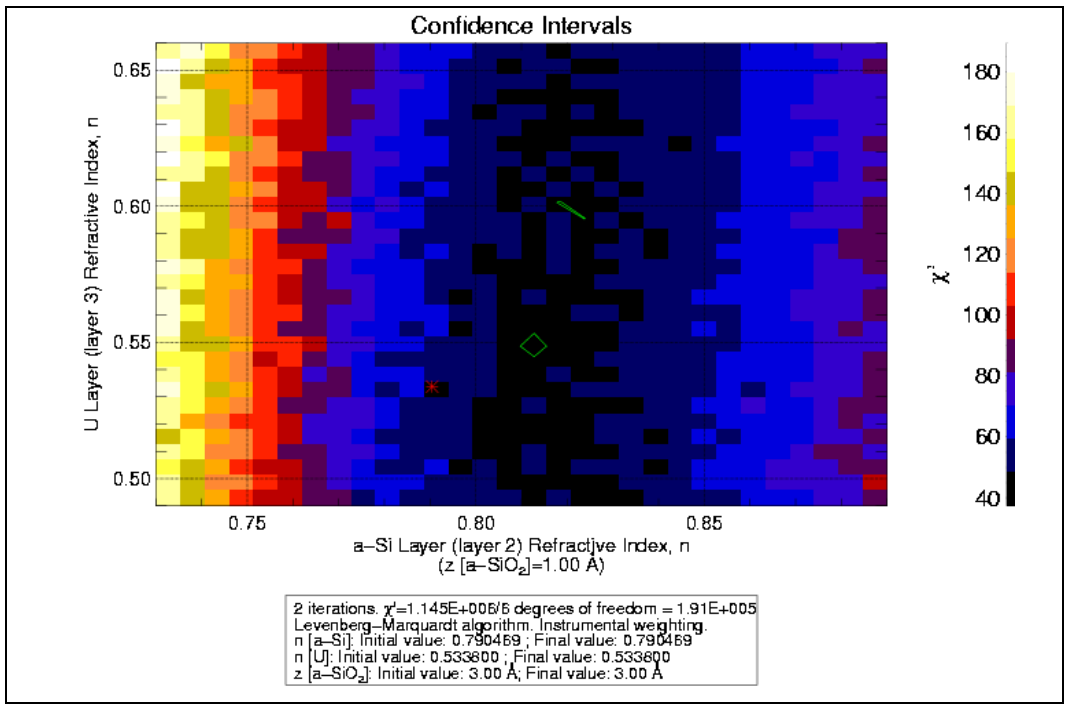

Figure 35: Confidence Integral of n for a-Si and U at 584 Å with amorphous silicon cap

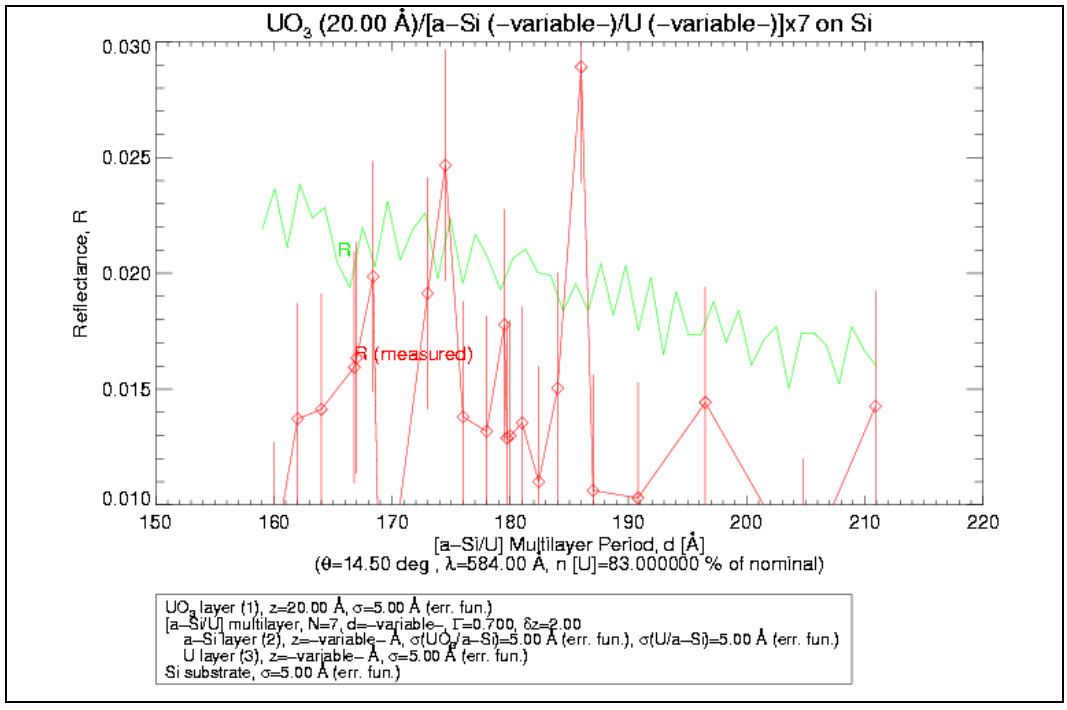

Figure 36: Fit n of a-Si and U at 584 Å with uranium oxide cap

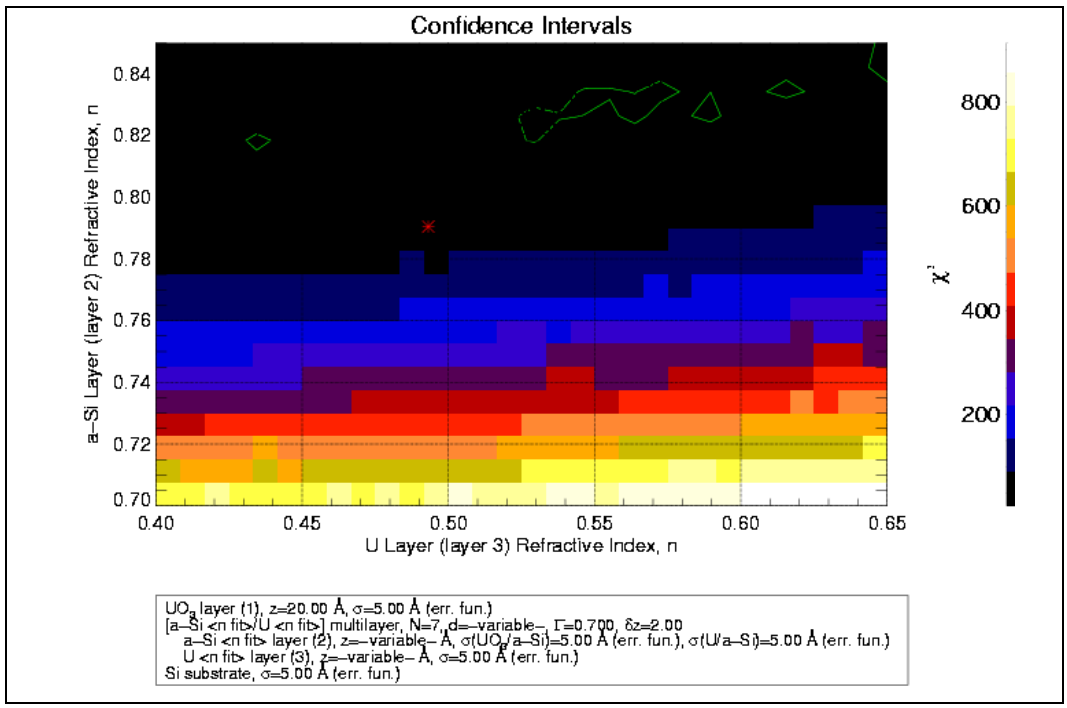

Figure 37: Confidence Integral of n for a-Si and U at 584 Å with uranium oxide cap

9 Conclusions

The IMAGE mission mirrors were designed using a trial and error method because the optical constants of U and a-Si were not well known. I have calculated the direction and magnitude the optical constants of U and a-Si and 304 and 584 Å should shift from reflectivity measurements of multilayer mirror coatings. The change in the optical constants at 304 Å was not large but it was significant. The change in the optical constants at 584 Å was significant but the significance and extent of the shift are not known. Because of the large differences at 584 Å the effect of the top layer of uranium oxide may play a stronger role than previously thought. The effects of the oxide layer could be eliminated by an ultra high vacuum system that is capable of deposition and measurement without exposure to oxygen and nitrogen.

The questions still exists does chemical bonding affect the optical properties in the EUV. There is some mechanism that is affecting the optical properties of U and a-Si at 304 and 584 Å that is not well understood. The difference may be due to measuring the reflectivity of multilayers that depend on the properties of different materials. One solution would be to measure the reflectivity of a single film and calculate the optical constants from reflectance data. An EUV ellipsometer is being developed at BYU and is another method to measure the optical properties of materials in the EUV.

Fitting was another area of difficulty in determining the optical constants in this thesis. Some of the fitting problems come from the small data set, and small range of layer thickness. This could be overcome by making more samples, but a faster and more economical solution would be to design a chamber that would be able to make measurements at many different angles as well as wavelengths. This would only require one film or multilayer that could be measured at many angles and provide a larger data set. A more robust and intelligent fitting algorithm would also increase the ability to obtain optical constants. This is another area of research at BYU that could significantly contribute to the determination of optical constants in the EUV.

This conclusion points to the design and fabrication of a chamber that will measure reflectivity of a sample as a function of angle, and possible in situ deposition of thin films. The development of a more robust fitting algorithm will also be an important step to accurately determine the optical constants of materials in the EUV.

References

[1] Brian G. Peterson, Hans K. Pew. LSMM A multilayer reflectivity calculation program using a matrix algorithm, Brighan Young University , circa 1984.

[2] B.L. Henke, E.M. Gullickson, and J.C. Davis. X-ray interactions: photoabsorption, scattering, transmission, and reflection at E=50-30,000 eV, Z=1–92, Atomic Data and Nuclear Data Tables, July 1993, 54,(no.2):181-342.

[3] Edward D. Palik ed. Handbook of Optical Constants of Solids, Academic Press Handbook Series, 1985.

[4] Edward D. Palik ed. Handbook of Optical Constants of Solids II, Academic Press Handbook Series, 1985.

[5] Matthew B. Squires, David D. Allred, R. Steven Turley. Will the real optical constants please stand up: Problems in obtaining optical constants for materials in the VUV, 4th International Conference on the Physics of X-Ray Multilayer Structures, Village of Breckenridge Resort, March 1–5, 1998.

[6] Adam M. Fennimore. Morphology and oxidation of U/Al and UN/Al multilayer mirrors, Honors Thesis, Brigham Young University, February 1998.

[7] Matthew B. Squires, David D. Allred, R. Steven Turley, David P. Balogh. Optical response of sputtered U and Si thin films and their native oxides in the EUV, APS Four Corners Section Meeting, Brigham Young University, October 16–17, 1998.

[8] David Griffiths. Introduction to Electrodynamics, Prentice-Hall Inc., 1981.

[9] Grant R. Fowles. Introduction to Modern Optics Second Edition, Dover Publications, 1989.

[10] F. Bassani, M. Altarelli, Interaction of Radiation with Condensed Matter, Handbook and Synchrotron Radiation. Vol. I, North-Holland Publishing Co., 1983.

[11] Milton Ohring, The Material Science of Thin Films, Academic Press, 1992.

[12] Philip R. Bevington. Data Reduction and Error Analysis for the Physical Sciences, McGraw-Hill Book Co., 1969.